Alexander B. Neiman and David F. Russell
J Neurophysiol 92:492-509, 2004. First published Oct 22, 2003; doi:10.1152/jn.00742.2003

You might find this additional information useful...

This article cites 77 articles, 23 of which you can access free at:
http://jn.physiology.org/cgi/content/full/92/1/492#BIBL

This article has been cited by 1 other HighWire hosted article:
Global Electrosensory Oscillations Enhance Directional Responses of Midbrain Neurons in Eigenmannia
J. U. Ramcharitar, E. W. Tan and E. S. Fortune
J Neurophysiol, November 1, 2006; 96 (5): 2319-2326.
[Abstract] [Full Text] [PDF]

Updated information and services including high-resolution figures, can be found at:
http://jn.physiology.org/cgi/content/full/92/1/492

Additional material and information about ***Journal of Neurophysiology*** can be found at:
http://www.the-aps.org/publications/jn

This information is current as of June 27, 2007 .

Journal of Neurophysiology publishes original articles on the function of the nervous system. It is published 12 times a year (monthly) by the American Physiological Society, 9650 Rockville Pike, Bethesda MD 20814-3991. Copyright © 2005 by the American Physiological Society. ISSN: 0022-3077, ESSN: 1522-1598. Visit our website at http://www.the-aps.org/.

Downloaded from jn.physiology.org on June 27, 2007

J Neurophysiol 92: 492–509, 2004;
10.1152/jn.00742.2003.

Two Distinct Types of Noisy Oscillators in Electroreceptors of Paddlefish

Alexander B. Neiman[1] and David F. Russell[2]

[1,2]*Center for Neurodynamics,* [1]*Department of Physics and Astronomy, and* [2]*Department of Biology, University of Missouri at St. Louis, St. Louis, Missouri 63121-4499*

Submitted 31 July 2003; accepted in final form 10 October 2003

Neiman, Alexander B. and David F. Russell. Two distinct types of noisy oscillators in electroreceptors of paddlefish. *J Neurophysiol* 92: 492–509, 2004; 10.1152/jn.00742.2003. Our computational analyses and experiments demonstrate that ampullary electroreceptors in paddlefish (*Polyodon spathula*) contain 2 distinct types of continuously active noisy oscillators. The spontaneous firing of afferents reflects both rhythms, and as a result is stochastically biperiodic (quasiperiodic). The first type of oscillator resides in the sensory epithelia, is recorded as approximately 26 Hz and ± 70 μV voltage fluctuations at the canal skin pores, and gives rise to a noisy peak at $f_e \approx 26$ Hz in power spectra of spontaneous afferent firing. The second type of oscillator resides in afferent terminals, is seen as a noisy peak at $f_a \approx 30$–70 Hz that dominates the power spectra of spontaneous afferent firing, and corresponds to the mean spontaneous firing rate. Sideband peaks at frequencies of $f_a \pm f_e$ are consistent with epithelia-to-afferent unidirectional synaptic coupling or, alternatively, nonlinear mixing of the 2 oscillatory processes. External stimulation affects the frequency of only the afferent oscillator, not the epithelial oscillators. Application of temperature gradients localized the f_e and f_a oscillators to different depths below the skin. Having 2 distinct types of internal oscillators is a novel form of organization for peripheral sensory receptors, of relevance for other hair cell sensory receptors.

INTRODUCTION

Oscillatory activity has been observed in several types of peripheral sensory receptors of vertebrates. Cold receptors produce bursts when chilled (Heinz et al. 1990). Odorants evoke synchronized oscillations in populations of olfactory receptor neurons in catfish (Nikonov et al. 2002). The membrane potential and hair bundles of auditory and vestibular hair cells of turtles, eels, and frogs can undergo spontaneous oscillations (Crawford and Fettiplace 1980, 1985; Martin et al. 2001, 2003; Rüsch and Thurm 1990). The mammalian ear may employ a "cochlear amplifier" involving basilar membrane oscillations driven by outer hair cells, to increase sensitivity and frequency selectivity (Eguíluz et al. 2000). Nonmammalian vertebrates may achieve similar amplification using oscillations in single auditory hair cells (Camelet et al. 2000; Manley 2001; Manley et al. 2001; Martin and Hudspeth 1999; Ospeck et al. 2001). Such oscillatory processes indicate that these sensory receptors are complex systems, acting as stimulus preprocessors with nonlinear properties.

The sensory epithelia of ampullary electroreceptors of marine cartilaginous fishes (ampullae of Lorenzini; see Zakon 1986) produce oscillations, like other hair cell receptors cited above. These are *self-sustained* (continuously ongoing) transepithelial oscillations at 10–35 Hz, depending on temperature, which can be recorded as voltage or current fluctuations in the canals leading from skin pores to sensory epithelia (Clusin and Bennett 1979a,b; Lu and Fishman 1995). However, Broun and Govardovskii (1983) and others have disputed the existence and significance of the epithelial oscillations, regarding them as artifacts of reducing the electrical loading on the epithelia, as when the skin is raised into the air (Bennett 1967; Obara and Bennett 1972).

The axon terminals of certain sensory afferents possess a different type of oscillatory mechanism, implicated in the bursting discharges of mammalian cold receptors (Bade et al. 1979; Darian-Smith et al. 1973; Heinz et al. 1990) and in the periodicity of afferent firing in ampullary electroreceptors of catfish (Schäfer et al. 1995) and dogfish sharks (Braun et al. 1994). The hypothesized oscillator has been modeled (Braun et al. 2000; Feudel et al. 2000) as arising from slow ion channels in the membranes of afferent terminals, giving rise to approximately 50-Hz waves of membrane potential, tending to drive periodic firing. Different modes of afferent firing (tonic, doublet, bursting) have been attributed to the dynamics of the slow ion channels. Membrane potential oscillations in somata of primary sensory neurons have been used as a model for events in afferent terminals (Amir et al. 2002).

In this report, we demonstrate 2 distinct types of oscillatory processes in the ampullary electroreceptors (ERs) of paddlefish (*Polyodon spathula*). These primitive fish have thousands of ERs on their rostrum, a flattened antennal structure projecting anterior of the head, as well as on the head and gill covers. As diagrammed in Fig. 1*A*, the receptive field of an ER afferent consists of a cluster, usually only one, of skin pores on the rostrum. Short (about 0.2 mm) canals lead from the skin pores to sensory epithelia composed of hair cells and support cells. Based on their ultrastructure (Jørgensen et al. 1972) and their polarity sensitivity of being excited by cathodal stimuli (Wilkens et al. 1997), paddlefish ERs are similar to the ampullae of Lorenzini of marine elasmobranch fishes (Zakon 1986) and to the ERs of sturgeon (Jørgensen 1980; Teeter et al. 1980). The polarity sensitivity implies that external electric fields are presumably sensed by the apical membranes of hair cells (Bennett and Obara 1986). From their basolateral membranes, the hair cells synaptically excite the terminals of primary afferents by ribbon synapses. Each cluster is innervated by 2–4 afferents (Russell et al. 2003). A primary afferent fires continuously ("spontaneously") at a nearly fixed frequency in the range of 30–70 Hz, varying for different afferents, fish, and temperatures. Afferent axons form the large anterior lateral line nerve (ALLn) on each side (Norris 1925), which enters the dorsal octavolateralis nucleus of the medulla for CNS processing of electrosensory information (New and Bodznick 1985). Affer-

Address for reprint requests and other correspondence: A. B. Neiman, Dept. of Physics and Astronomy, Ohio University, Athens, OH 45701.

The costs of publication of this article were defrayed in part by the payment of page charges. The article must therefore be hereby marked "*advertisement*" in accordance with 18 U.S.C. Section 1734 solely to indicate this fact.

 0022-3077/04 $5.00 Copyright © 2004 The American Physiological Society

Downloaded from jn.physiology.org on June 27, 2007

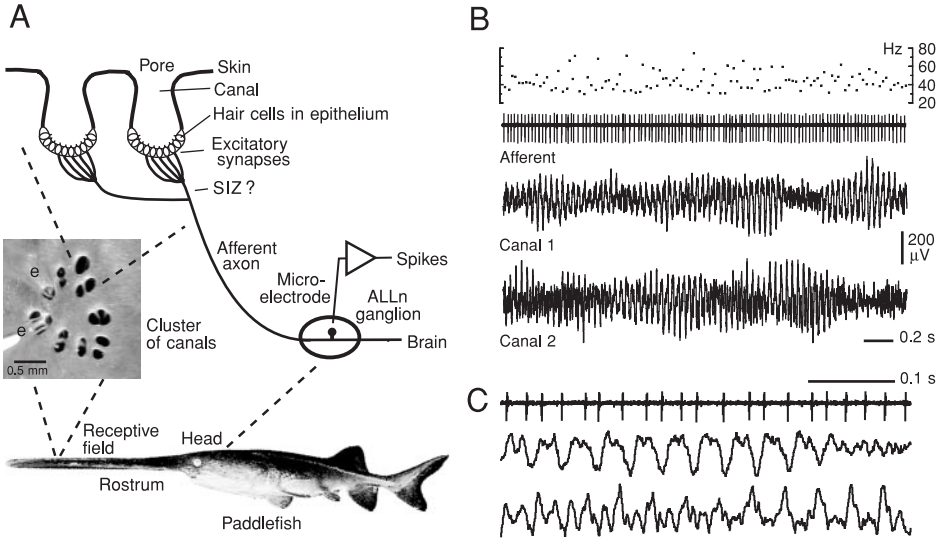

FIG. 1. Background activity of electroreceptors. *A*: diagram of an electroreceptor in paddlefish. SIZ, presumed spike initiating zone. e, photo of pipette electrodes in 2 canals of one large cluster, which was the receptive field of the afferent in *B* and *C*. An afferent innervates all the sensory epithelia in a cluster. *B*: raw recording of the spontaneous firing of an electroreceptor afferent, with its instantaneous firing frequency (*top trace*) and simultaneous pipette recordings from 2 canals. Mean firing rate was 42.5 Hz. *C*: expanded segment showing canal oscillations at 26.7 Hz (*middle trace*) and 53 Hz (*bottom trace*, *left*). Positive signal polarity is shown upward for all traces, referred to the environmental water.

ents respond best to external sine-wave stimulus frequencies of 1–10 Hz, maximally at about 5 Hz, with declining sensitivity out to 0.1–30 Hz (Pei et al. 1998; Wilkens et al. 1997). Threshold has been estimated from behavioral tests as approximately 0.5 μV/cm (Russell et al. 1999, 2001). The ERs form a passive sensory system used for detection and capture of planktonic prey (Russell et al. 2001; Wilkens et al. 1997) and avoidance of metal obstacles (Gurgens et al. 2000). Kalmijn (1974) demonstrated that paddlefish avoid electric dipoles.

We present computational and experimental evidence that paddlefish ERs have a population of around 25-Hz noisy oscillators in their sensory epithelia, along with a 30- to 70-Hz pacemaker-like oscillator in each afferent terminal (Neiman and Russell 2001). Both types of oscillators affect the firing of primary afferents, resulting in stochastic biperiodic output, normally showing both fundamental frequencies. An advantage of the paddlefish electroreceptor system is that it permits simultaneous recording from sensory epithelia and single afferents, which allowed us to study interactions of the epithelial and afferent oscillators. Such dual data are unavailable for other types of hair cell–primary afferent receptors. In sum, we have recognized a novel type of organization for a sensory receptor, of having 2 different types of embedded oscillators. Our findings illustrate that peripheral sensory receptors of vertebrates can be surprisingly complex nonlinear systems. Our findings are of general interest for understanding the roles of oscillations in other sensory receptors (e.g., the hair cell–primary afferent receptors for hearing and balance).

METHODS

Experimental

Paddlefish were obtained from the Missouri Dept. of Conservation, and raised in large aquaria at 23–27°C. The data were from in vivo experiments on 20 paddlefish, of 37.3 ± 4.4 cm total length, and 12.8 ± 1 cm rostrum length. A protocol for these experiments was approved by the institutional animal care and use committee. The protocol called for a fish to be anesthetized during surgery with 3-aminobenzoic acid ethyl ester methanesulfonate (0.1 g/l). The fish was immobilized with 0.6 mg curare administered intramuscularly. It was artificially ventilated with dechlorinated tap water of 500–600 μS/cm conductivity, bubbled with 100% O_2, flowing into the mouth by gravity from an elevated reservoir. An in-line chiller regulated the water temperature at about 22°C. Water hoses were routed so as to minimize the loop area of the water circuit. The fish was in an elongated 6 × 15 × 55 cm (H × W × L) all-plastic experimental chamber, in water about 5 cm deep. The entire rostrum was always submerged under 5–10 mm of water, such that there was normal electrical loading on the ERs. The chamber was on an air-support vibration-damping table, inside a Faraday cage made of ferrous hardware cloth. The plastic braces holding the fish did not compromise the skin, and did not compress the rostrum, important for maintaining its blood supply. Water motion around the rostrum was attenuated by partitioning the chamber transversely, at the base of the rostrum, with a slab of electrically conductive 2% wt/vol agarose. The sensory ganglion of an ALLn was exposed, lateral to the medulla, and a 12-MΩ tungsten microelectrode was advanced into the ganglion to obtain single-unit recordings of afferent spikes. To insulate electrically the body interior from the water, the water level was adjusted to have the cranial opening in air; petroleum jelly was applied topically to the skin around the opening; and saline flow onto the brain was discontinued during data collection. A 50 × 50-mm chlorided silver plate under the head led to system ground.

A unit's modality as an electroreceptor, and the location of its receptive field, were established by presenting 5-Hz sinusoidal electrical stimuli from a 2.5-mm local dipole electrode, connected to a battery-powered constant-current linear stimulus isolation unit. The isolator's internal noise was 0.1 nA rms over the relevant 0.1- to 100-Hz band. Recordings of oscillatory potentials from a canal were made by pressing a heat-polished glass pipette filled with water, having a tip diameter of 150–200 microns, into a canal opening at the skin. Spikes and canal signals were digitized at 20–22 kHz and 5–16 kHz, respectively, using an interface and Spike2 software from Cambridge Electronic Devices (Cambridge, UK).

Data analyses to detect and characterize oscillations

All the data presented here were from fresh in vivo preparations <16 h old. Values are stated as means ± SD. Kolmogorov–Smirnov (K-S) statistical tests were run using Systat v.9 software. P_{H_0} refers to the probability of the null hypothesis in statistical tests.

Afferent spike times were derived off-line using Spike2 software to identify the peaks or troughs of digitized action potentials, by fitting parabolas, interpolating between samples to a time resolution of 5 μs. As a result, a sequence of spike times t_n, $n = 1, \ldots, N$, was obtained. The total number of afferent spikes N in a 5- to 30-min data recording was $1–8 \times 10^4$. The single-unit nature of such afferent recordings was

Downloaded from jn.physiology.org on June 27, 2007

indicated by similar shapes and heights of spikes, and by the lack of interspike intervals (ISIs), $T_n = t_{n+1} - t_n$, shorter than 5 ms.

Several types of time series analyses were used to detect and characterize oscillations and noise in ERs, using custom software programmed in Fortran77 and run on a Sun workstation, or programmed in the Spike2 script language and run on a PC. Most time series analyses require that data be stationary (i.e., have consistent properties) over the duration of a recording. To minimize nonstationarity, our analyses were applied to data segments 200–900 s in length, in which a simple moving average of the afferent firing rate over a 10-s window fluctuated less than ±2% from the mean rate for the data, and showed no trend, and in which the instantaneous firing rate revealed no gaps or unusual transients.

The coefficient of variation (CV, dimensionless) of afferent firing, a widely used measure of variability, was calculated as the SD of ISIs divided by the mean ISI: $CV = \sqrt{\text{var}\,[T_n]}/\langle T_n \rangle$, where *var* is the variance and angled brackets denote averaging. The *mean firing frequency* ($\bar{f}$) in a data segment was calculated from the time between the first and last spike. As computational controls, renewal processes were generated from spike time series by repeatedly shuffling the order of ISIs (shuffled surrogates; Dolan et al. 1999). Shuffling did not alter the ISI histogram. Renewal processes have no memory, such that each ISI is uncorrelated with earlier or later ISIs.

Power spectra of afferent spike trains were calculated as in Douglass et al. (1993) and Gabbiani and Koch (1998). A spike train was represented as a sequence of delta-like functions centered at the spike times: $a(t) = \sum_{n=1}^{N} \delta(t - t_n)$ A list of spike times was converted into a sampled waveform having a baseline value of "0", assigning to a single sample nearest to each spike time the value $1/\Delta t$, where Δt is the sample interval (usually 50 μs). The power spectrum of this series of delta functions was calculated from overlapping windows, usually of size $w = 2^{18}$ samples, applying a raised-cosine window filter. Power was normalized to the mean number of spikes per window $\eta = \bar{f}\, w \Delta t$, to have similar scaling for different afferents, yielding units for power spectral density (PSD) of: $(\text{spikes/s})^2/(\text{spike Hz}^{-1})$. We usually displayed spectra with logarithmic vertical scales and assigned units of −dB relative to the maximum.

The *center frequency* f_0 of a power spectrum peak was estimated by bisecting the peak area if it was asymmetrical, or by fitting Lorentzians for a sharp symmetrical peak, $S(f) = c/[(f - f_0)^2 + d^2]$, where c and d are parameters to be fitted. The *width of a peak* Δf_{50} was calculated as $\Delta f_{50} = 2d$, or was measured at 50% of its maximum above an estimated baseline (from linear spectra, after minimal smoothing). The *quality factor* of a spectral peak was calculated as $Q = f_0/\Delta f_{50}$. The quality factor is widely used to describe the sharpness of a peak; higher values correspond to sharper peaks.

The *coherence function* is useful for characterizing the correlation properties of 2 stochastic processes in the frequency domain (see Gabbiani and Koch 1998). We used it to look for corresponding oscillations in canal and afferent activity. Coherence ranges from 0 (none) to 1 (maximal coherence). The coherence function $\Gamma(f)$ was calculated as the ratio of the square of the absolute value of the cross-spectrum of a canal signal and corresponding spike train, to the product of their power spectra (Bendat and Piersol 2000): $\Gamma(f) = |S_{as}(f)|^2/[S_{aa}(f) S_{ss}(f)]$, where $S_{as}(f)$ is the cross-spectrum and $S_{aa}(f)$, $S_{ss}(f)$ are the power spectra of the afferent spike train $a(t)$ and the canal signal $s(t)$, respectively.

An alternate approach to analyzing the oscillatory firing patterns of ER afferents, which does not rely on power spectral analysis, was to map the *phase angles* $\phi(n)$ (Glass and Mackey 1988; Janson et al. 2001) between sequential pairs of ISIs, from return maps (below). In any oscillatory system, it is possible to represent the periodicity as a map of observed and preferred values ("attractors") in a multidimensional phase space. Phase angles measure the "rotation" (if any) of vectors connecting sequential points in a return map of afferent ISIs, around a center, $\phi(n) = \arctan[(T_{n+1} - \langle T_n \rangle)/(T_n - \langle T_n \rangle)]$. If an afferent's firing has 2 independent frequencies (i.e., is biperiodic), plots of $\phi(n + 1)$ versus $\phi(n)$ should exhibit invariant curves (attractors), as the projection of a 2D torus, given that the phases of 2 oscillators give the 2 angles needed to describe a torus. If there is a rational (integer) relation between the frequencies of 2 oscillators, then the phase angle map should demonstrate "fixed points" (i.e., loci) where the values cluster. If there is only one oscillatory component to an afferent's firing, a phase angle map with no structure (uniform distribution of points) would be predicted.

The normalized *cross-correlation* function $G(\tau)$ was used to characterize statistical relations between signals recorded from 2 canals, and was calculated as follows: $G(\tau) = \langle [s_1(t) - \langle s_1 \rangle][s_2(t + \tau) - \langle s_2 \rangle] \rangle / \sqrt{\text{var}\,(s_1)\,\text{var}\,(s_2)}$, where τ is the time lag and angled brackets stand for averaging over time t. $G(\tau)$ ranges from +1 (completely correlated) to zero (no correlation) to −1 (completely anticorrelated), and is a sensitive measure.

The correlation properties of sequences of ISIs were analyzed using 2 approaches. *Return maps* plotted an interval T_n against the subsequent interval T_{n+1}, in a pairwise manner. The dynamics of correlations over longer sequences of ISIs were revealed using the normalized autocorrelation function of ISIs, also known as the *serial correlation coefficient* $C(k)$, $C(k) = (\langle T_{n+k} T_n \rangle - \langle T_n \rangle^2)/\text{var}\,[T_n]$, where k is the lag after a given ISI expressed as the number of elapsed ISIs (Tuckwell 1988). $C(k)$ ranges from +1 (complete correlation) to zero (lack of correlation) to −1 (complete anticorrelation). A renewal point process (e.g., from randomly shuffling the order of ISIs) shows no correlations between event intervals, such that $C(k) = 1$ for $k = 0$ (that is, an ISI is correlated with itself) and $C(k) = 0$ for $k \neq 0$.

The *reverse correlation* [revcor, $R(\tau)$] reveals an average stimulus (canal signal, in our case) occurring before spikes (see Gabbiani and Koch 1998). We applied revcor analysis to paired recordings from canal and afferent. Pretriggered averaging was carried out on canal signals, using as a timing reference the afferent spikes recorded at the ALLn ganglion near the brain. This was equivalent to calculating $R(\tau) = (1/N) \sum_{n=1}^{N} s(t_n - \tau)$, where τ is the lead or lag time relative to spike times t_n.

Coupling of afferent firing to canal oscillations was also revealed by statistical analysis of their relative timing, using the concept of an analytic signal and the *Hilbert transform* (Bendat and Piersol 2000; Pikovsky et al. 2001). If there is no interaction (coupling) between these 2 processes, then there should be no preferred phase, and thus a uniform distribution is expected; otherwise, if there is coupling, the phase distribution must exhibit a peak at a preferred phase. Each cycle of canal oscillation was considered as 2π radians, and the probability density of the relative instantaneous phase of the canal oscillation at each afferent spike (φ_P) was calculated. The complex analytic signal $z(t)$ was constructed, with the real part being the original canal signal and the imaginary part being its Hilbert transform: $z(t) = s(t) + i s_H(t) = A(t) e^{i\varphi(t)}$, where $A(t)$ and $\varphi(t)$ are the instantaneous amplitude and phase, respectively, and $s_H(t)$ is the Hilbert transform of the canal signal $s_H(t) = (1/\pi) \int_{-\infty}^{+\infty} [s(u)/(t - u)]/du$. The instantaneous phase $\varphi(t)$ is the argument of the analytic signal, and was calculated at each afferent spike, $\varphi_P = \varphi(t = t_n)$.

The frequency response of an ER afferent was measured using *stimulus reconstruction* (Bialek et al. 1991; Gabbiani and Koch 1998). A long (10-min) broadband Gaussian noise stimulus waveform $\xi(t)$ was applied to an ER. This stimulus was then estimated from the ER afferent firing using optimal Wiener–Kolmogorov filtering (Bendat and Piersol 2000) of the spike train. The optimal filter with the response function $h(t)$ was applied to each spike to give an estimate of the stimulus: $\xi_{est}(t) = \sum_{n=1}^{N} h(t - t_n)$. The response function of the filter is given in the frequency domain by $h(f) = S_{\xi a}(-f)/S_{aa}(f)$, where $S_{\xi a}(f)$ is the cross-spectrum of the stimulus noise and the afferent spike train and $S_{aa}(f)$ is the power spectrum of the afferent spike train. The encoding capacity of an ER was then judged from the effective noise, the difference between the original and estimated stimulus: $e(t) = \xi(t) - \xi_{est}(t)$. The signal-to-noise ratio (SNR) at

Downloaded from jn.physiology.org on June 27, 2007

different frequencies was calculated as the ratio of the stimulus power spectrum to the power spectrum of the effective noise, $SNR(f) = S_{\xi\xi}(f)/S_{ee}(f)$. The SNR as a function of frequency equals 1 when there is no encoding, and attains large values for good encoding.

Thermal gradients

Focal streams of water were used to create temperature gradients through the rostrum, taking advantage of its thin planar geometry. Thermally evoked changes in the frequency of spontaneous firing were analyzed for afferents from visible receptive fields on the dorsal surface of the rostrum. The water flowed by gravity onto a receptive field, through 4-mm ID nozzles, at 350 ml/min, from elevated reservoirs containing oxygenated water already chilled or heated to the desired temperature. The high flow rate ensured good temperature control. In some experiments, a second nozzle was positioned underneath the receptive field, to direct water vertically upward onto the ventral surface of the rostrum. Tubing from the nozzles led to plastic valves, including a latching solenoid valve that was energized only momentarily and so did not heat the water. The temperature was monitored using an electronic thermometer with a thin plastic-coated short-latency probe placed near the skin receiving a flow of water. Because the data (i.e., afferent spike times) were nonstationary, afferent power spectra were represented as time-evolution waterfall displays, using DISLIN software (DISLIN) to code power spectral density (scaled as dB) as colors, such that red/blue represent high/low power, respectively.

A steady laminar flow of ambient-temperature water directed orthogonally down onto a receptive field had little or no effect on an afferent's background firing. However, pulsatile water flow was strongly stimulatory, and so we took steps to minimize pulsations, including immobilizing the water tubing and nozzle, gravity flow of water from elevated reservoirs, and the use of a latching solenoid valve to switch rapidly between 2 sources of water (at different temperatures) such that water flowed continuously onto a receptive field.

RESULTS

This report demonstrates and characterizes 2 separate types of oscillators embedded into the structure of paddlefish electroreceptors (ERs), and explores the functional implications of this biperiodic organization. Our hypothesis is that each sensory epithelium contains a population of approximately 25-Hz oscillators, whereas each afferent terminal contains a separate 30- to 70-Hz oscillator. Because the sensory epithelia synaptically excite the afferent terminals, an ER represents a system of coupled oscillators, whose output reflects both types of oscillations, and is biperiodic (quasiperiodic) as a result. We first characterize the background ("spontaneous") activity of paddlefish ERs. Several types of experimental studies on the responses of ERs to external perturbations are then presented, in the context of demonstrating and localizing the oscillators. Finally, we explore some of the functional consequences of biperiodic organization for the operation of ERs.

Spontaneous activity with two fundamental frequencies

We studied the spontaneous activity of ERs because its stationarity is a prerequisite for applying analytical approaches from time series analysis and nonlinear dynamics to look for oscillatory processes. Spontaneously active biological oscillators fall within the general class of so-called self-sustained oscillators, a type of dynamical system defined mathematically, exhibiting stable oscillations whose amplitude and frequency depend on *internal* parameters of the system rather than on initial conditions. Self-sustained oscillators are inherently nonlinear, and so approaches from nonlinear physics are valuable and appropriate for characterizing them (see, e.g., Anishchenko et al. 2002; Strogatz 1994).

Figure 1*B* illustrates the spontaneous activity of paddlefish ERs. Spontaneous noisy voltage oscillations at about 25 Hz were always present in recordings made with water-filled glass pipettes inserted partway into receptor canals (Fig. 1*B*, *canal traces*), in healthy preparations <16 h old. Such "canal oscillations" had rms amplitudes of 15 ± 6 μV, ranging from 7 to 33 μV, and a mean peak–peak amplitude of about 140 μV (i.e., ±70 μV), ranging from 65 to 350 μV (for 42 canals from 5 fish at about 22°C). The amplitude of oscillations waxed and waned on a time scale of a few seconds, following different time courses in different canals. Their frequency could switch between the fundamental mode at about 25 Hz and harmonics at 2× or 3× higher frequencies (Fig. 1*C*, *bottom canal trace*).

The primary afferents from paddlefish electroreceptors fired continuously in the absence of external stimulation (Fig. 1*B*, *afferent trace*). The mean firing frequency $\bar{f}$ was 54.1 ± 8.5 Hz (range 27.6–69.1) for 39 afferents from 16 fish at controlled temperature (22.0 ± 0.61°C). The instantaneous firing rate was characteristically irregular in fresh preparations, varying 2- to 3-fold, giving coefficients of variation of the ISIs of 0.19 ± 0.06 (range 0.10–0.38, mode 0.17, for 39 afferents). Spike doublets occurred frequently (Fig. 1*C*). Fluctuations in an afferent's firing rate on slower time scales were revealed by computing moving averages using a sliding window. The firing rate fluctuated around a mean, usually with no net trend over the several hours' duration of a recording. Because data must be stationary for most time series analyses, we applied the criteria that there should be no net trend of an afferent's firing rate and that, in moving averages with a 10-s sliding window, the firing rate should fluctuate less than ±2% from the mean rate for the data segment.

PROPERTIES OF SPONTANEOUS CANAL OSCILLATIONS. The voltage fluctuations we recorded from a canal appeared to be summed field potentials from a population of similar oscillators in the canal's sensory epithelium. Power spectra of canal signals (Fig. 2*A*) always showed a fundamental peak at a center frequency f_c = 25.5 ± 1.6 Hz (range 22.6–27.5, for 25 canals from 4 fish at 21.5–21.9°C). There was always a long series of higher harmonics at integer multiples of f_c, which declined in power and increased in width and symmetry at higher frequency, as expected for nonlinear stochastic oscillators. The oscillation frequencies were remarkably similar in simultaneous recordings from pairs of canals (Fig. 2*A*): the difference in f_c was 0.06 ± 0.37 Hz for 18 pairs of canals from 5 fish, not significantly different from zero (*t*-test). In a few canals, the fundamental f_c peak was fractionated into 2 or 3 subpeaks. Sometimes there was an additional broad peak in power spectra of canal signals, in the range of 10–28 Hz.

Histograms of the sample values from canal recordings formed bell-shaped distributions (Fig. 2*B*), which were accurately Gaussian in some cases [e.g., $P_{H_0} > 0.95$ (K-S test) when comparing the *black trace* in Fig. 2*B* to a theoretical Gaussian of identical SD = 15.1 μV]. This is consistent with the oscillations recorded from a canal arising from a population of similar but uncorrelated generators (see DISCUSSION).

We did several control experiments to exclude alternate

Downloaded from jn.physiology.org on June 27, 2007

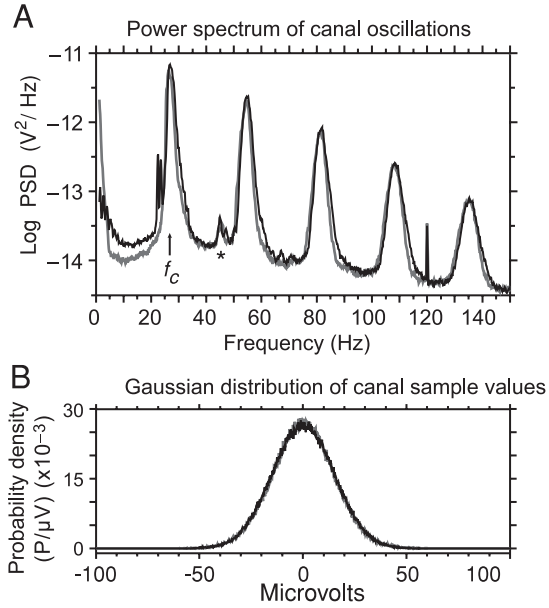

FIG. 2. Canal oscillations. *A*: power spectra for 2 canals (*black*, *gray traces*) recorded simultaneously and superimposed. Canal signals were sampled at 11.1 kHz, and high-pass filtered electronically at about 0.5 Hz. f_c, center frequency of the fundamental peak. PSD, power spectral density; the units refer to volts at the canal. Transient at 120 Hz was interference. Asterisk: minor peak was attributed to attenuated afferent spikes. *B*: superimposed Gaussian probability density distributions of 3×10^4 sample values from 5-min recordings from the same 2 canals (*black*, *gray traces*) as in *A*, after low-pass digital filtering at 205 Hz, setting each mean to zero, and decimating to a sample rate of 1,110 Hz.

explanations for the canal oscillations. *1*) Lifting the pipette tips into the water >5 mm above the skin abolished the oscillations. *2*) The canal oscillations persisted while the ventilatory water flow was stopped briefly. *3*) Similar canal oscillations were observed when the water chiller was not installed, or when the recirculation pump was switched off. *4*) Pressing the pipette tip to the skin gave only low-frequency noise, having a power spectrum resembling $1/f$ noise.

Lack of correlation between canal pairs. When the normalized cross-correlation function $G(t)$ (see METHODS) was calculated between signals from pairs of canals of the same cluster (i.e., same receptive field), the cross-correlation was negligible: $|G| < 0.015$. For comparison, cross-correlations were calculated between canals of different clusters (i.e., different receptive fields), which had similar negligible magnitudes of about ± 0.015. The lack of cross-correlation shows that the oscillatory signals in different canals arise independently, even within the same receptive field, despite their remarkable similarity in frequency.

Noisiness of canal oscillations. Canal oscillations were obviously noisy. Several analyses were carried out to show that their noise (stochasticity) was attributed to fluctuations of both the instantaneous (cycle-by-cycle) frequency as well as the instantaneous amplitude. *1*) Instantaneous frequency was derived from the times between zero crossings of canal signals. Some canal recordings showed mainly the fundamental frequency f_c, whereas others dwelled in the $2f_c$ mode for extended times (as Fig. 1*C*, *bottom canal trace*). In a probability density plot of the instantaneous period (not illustrated), the half-maximum width of the fundamental peak was 2.4 ± 0.6 Hz for $n = 6$ canal recordings. Hence, within a given recording, the characteristic frequency of canal oscillations did vary about $\pm 5\%$ from the center f_c frequency. This was also indicated by the finite width of the f_c peak in canal power spectra (Fig. 2*A*); we measured $\Delta f_{50} = 1.8 \pm 0.3$ Hz for 10 canals from 2 fish, by fitting Lorentzians (see METHODS). *2*) The instantaneous peak-to-peak amplitude of canal oscillations was derived using the Hilbert transform (see METHODS; Bendat and Piersol 2000). Such amplitudes conformed well to a Rayleigh distribution (not illustrated), consistent with varying randomly (Bendat and Piersol 2000).

TWO FUNDAMENTAL FREQUENCIES IN POWER SPECTRA OF SPONTANEOUS AFFERENT FIRING. We made extensive use of power spectral analysis of afferent spike trains (see METHODS), because spectra provide detailed information in the frequency domain, are appropriate for studying oscillatory processes, and also reveal variability. Power spectra of long (5–15 min) stationary recordings of spontaneous afferent firing always showed a consistent pattern of peaks (Fig. 3*A*, *black trace*). The peaks are indicative of oscillatory processes because a spectral peak signifies periodicity. The narrow peak labeled "f_a" was usually the highest in power; we will present several

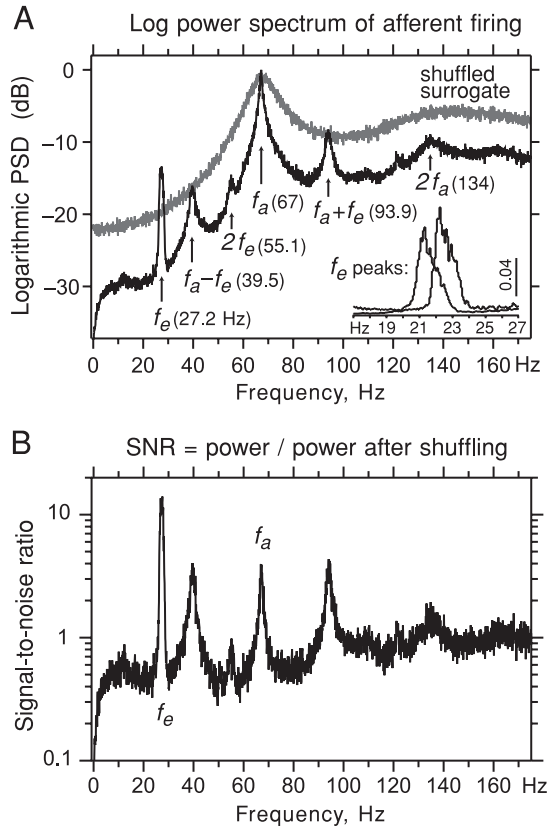

FIG. 3. Afferent power spectrum of spontaneous firing. No external stimulus was presented, pipette electrodes were not applied to canals, and the rostrum was completely immersed in water. *A*: *black trace*: spectrum is scaled logarithmically as dB relative to the maximum; data from 758-s firing, 50,532 spikes. f_a, afferent oscillator peak. f_e, epithelial oscillator peak. Each value in parentheses states the peak center frequency (Hz) at the arrow. PSD, power spectral density. *Inset*: expanded views of f_e peaks from 2 spectra, showing asymmetry. *A*: *gray trace*: logarithmic spectrum of same data after repeatedly shuffling the order of interspike intervals (ISIs). *B*: signal-to-noise ratio (SNR) at different frequencies was calculated by dividing the power values in *A* (*black trace*) by the shuffled values in *A* (*gray trace*), point by point. Baseline is lower at frequencies <100 Hz because of the presence of peaks.

Downloaded from jn.physiology.org on June 27, 2007

types of analyses and experimental data indicating that the f_a peak arises from a pacemaker mechanism in the afferent terminals. There was another narrow peak at 20–30 Hz, labeled "f_e"; we will show that the f_e peak corresponds to synaptic input to the afferent from the epithelial (canal) oscillators. Higher harmonics of f_a and sometimes f_e could be observed. Two minor sideband peaks at frequencies of $f_a \pm f_e$ were usually observed. In general, power spectra of spontaneous afferent firing had the structure expected for a periodically forced nonlinear oscillator. By this model, f_a is the natural frequency of the driven oscillator, f_e is the forcing frequency coming from a second oscillator, and the sideband peaks at $f_a \pm f_e$ are combination frequencies.

The f_a peak was often narrow and sharp. That is, the process giving rise to the f_a peak was strongly periodic, and therefore we describe it as an oscillator. The average width of the f_a peak at half-power (Δf_{50}) was 4.7 ± 5.6 Hz (for 45 afferents from 14 fish). The f_a peak was usually sharp, as measured by its large quality factor (see METHODS), $Q_a = 31 \pm 34$ ranging from $Q = 2$ to $Q = 166$. Nevertheless, the finite width and broad base of the f_a spectral peak means that the frequency of the underlying process fluctuated around a mean (i.e., was stochastic). The center frequency of the f_a peak was always similar to the mean firing rate $\bar{f}$ for that data segment; the mean difference between them was 0.01 ± 0.66 Hz for $n = 50$ afferents from 14 fish, which is not significantly different from zero (*t*-test). This close correspondence between f_a and $\bar{f}$ suggests that the f_a oscillator reflects properties of the afferent terminal and probably resides there, as in certain thermoreceptors (Bade et al. 1979; Braun et al. 2000) because the afferent terminal is where spikes are initiated.

The f_e peak was also relatively narrow, 1.7 ± 0.4 Hz in width at half-power, ranging from 0.8 to 2.6 Hz (for $n = 48$ afferents from 16 fish at 22 ± 1°C), similar to the width of the f_c peak in canal spectra. Again, such a sharp peak indicates periodic activity, and so we describe the f_e peak as arising from a stochastic oscillator (or a population thereof). The f_e peak was typically not symmetrical, and instead was often skewed toward lower frequencies, with tails (*inset*, Fig. 3*A*). Examples in which the f_e peak had 2 maxima were sometimes seen. The center frequency of the f_e peak was always similar to the frequency of canal oscillations, measured from the center frequency of the fundamental peak in canal power spectra (as Fig. 2*A*). The mean difference between them was −0.06 ± 0.47 Hz for $n = 42$ canal-afferent pairs from 7 fish, which is not significantly different from zero (*t*-test). This close correspondence between f_c and f_e suggests that the f_e oscillator(s) resides in the canals, specifically in the sensory epithelia, like the epithelial oscillators reported by Clusin and Bennett (1979a,b) and Lu and Fishman (1995). Our hypothesis is that the f_e peak in afferent power spectra reflects summed synaptic input to an afferent from populations of stochastic oscillators of similar frequency in the canal epithelia (the receptive field) converging onto the afferent. The f_e peak was always observed in afferent power spectra of fresh preparations, including when no pipette electrodes were applied to any canals.

Two sideband peaks at frequencies of $f_a \pm f_e$ signify coupling or nonlinear mixing of the oscillatory processes, resembling line splitting in the output of a heterodyne electronic circuit. The sidebands were most prominent when the f_a and f_e peaks were narrow and high-power. The sidebands are consistent with 2 alternate models: serial unidirectional coupling from the epithelial oscillators to the afferent oscillator, or parallel nonlinear mixing of the epithelial and afferent oscillatory processes at a downstream stage (see DISCUSSION).

This characteristic pattern of spectral peaks was lost after repeatedly shuffling the order of ISIs, to create a shuffled surrogate (Dolan et al. 1999) whose ISI histogram was unchanged. A power spectrum of the shuffled data (Fig. 3*A*, *gray trace*) still showed a peak at the mean firing rate $\bar{f}$, supporting our hypothesis that firing in the afferent terminal is basically driven by an oscillatory process. Because the other peaks were lost after shuffling, they reflect correlations in the data between sequences of ISIs.

The overall form of afferent power spectra resembled a ramp, rising with increasing frequency, and leveling off above about 120 Hz. This ramplike shape depends on how the spike time series is represented for purposes of calculating power spectra. We used a series of delta function approximations (see METHODS). Other representations (e.g., as a series of pulses, or as a telegraph waveform) give other global forms to power spectra of time series, while still showing a similar pattern of spectral peaks, characteristic of a given data set. To attempt to factor out the spectrum shape, we calculated a type of SNR ratio by dividing an afferent power spectrum by the power spectrum of the same data after shuffling. This gave an approximately flat baseline (Fig. 3*B*), with all the same peaks. The f_e peak had the highest SNR.

Control experiments. 1) It is important to note that for Fig. 3, the entire rostrum was completely submerged under 5–10 mm of water, and pipette electrodes were not applied to any of the canals, such that there was normal electrical loading on the canals (shunting to the surrounding water). This is important because some authors have regarded ER oscillations as artifacts of reduced canal loading (e.g., attributed to raising the skin into air) and have disputed the normalcy of ER oscillations. *2*) Our demonstration of the f_e peak in power spectra of spontaneous single-afferent firing demonstrates that the canal oscillations occur normally, given that this approach avoided the use of a pipette to record oscillations from a canal, which could alter its operation. *3*) We recorded the background firing of afferents while briefly stopping the flow of ventilatory water to the fish, yet maintaining a constant depth of water (about 5 cm) around the fish, and also switching off the recirculating water pump, chiller, and other nonessential equipment. The spike time series met criteria for stationarity for the initial 1–3 min, on the initial trials. Power spectra from afferents recorded under these conditions (not illustrated), including a pair of afferents recorded simultaneously, still showed all the same peaks as in Fig. 3, as evidence that the peaks are not artifacts of water flow noise, the water chiller, or other instruments. *4*) Another type of control experiment was to surround the rostrum in a close-fitting enclosure made of mu metal, to shield the electroreceptors from possible electrical or magnetic fields. The mu metal wall of the shield was coated to insulate it electrically from the water, but a wire connected the mu metal to system ground. After finding an afferent with a receptive field near the tip of a rostrum, the afferent recording was held while sliding the mu metal enclosure horizontally until the receptive field was 7–9 cm inside the enclosure. With the shield in place, long recordings of background afferent firing gave power spectra (not illustrated) resembling those in Fig. 3,

Downloaded from jn.physiology.org on June 27, 2007

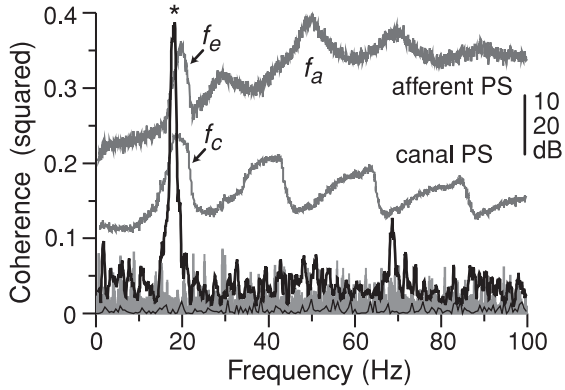

FIG. 4. Coherence function (*bold trace*) calculated between the power spectrum (PS) of an afferent's firing (*top gray trace*) and the power spectrum of oscillations in a canal in the receptive field (*bottom gray trace*), from simultaneous recordings of spontaneous activity. The coherence peak (asterisk) is evidence that the f_e frequency peak in afferent activity is driven by the canal oscillations. *Baseline, thin black trace*: surrogate control, in which the coherence peak near f_e was abolished after randomizing the phase of the canal signal while preserving its power spectrum (see text). *Baseline, gray shading*: control, showing lack of coherence between this afferent and a canal in a different cluster.

with all the same peaks. *5*) We were unable to reveal alternating electric currents in the chamber water at frequencies near f_e or f_a, using recording electrodes in the chamber water, connected to nerve preamplifiers. *6*) We also used a LakeShore model 420 Gaussmeter with a probe sensitive to 10^{-4} G, in different orientations inside the iron-screen Faraday cage, but it failed to reveal any oscillatory magnetic fields in the range of f_e or f_a. We conclude that the peaks in afferent power spectra are normal features of electroreceptor firing.

Coherence between canal and afferent. To confirm the close relationship between the natural frequency of canal oscillations (f_c) and the f_e peak in afferent power spectra, we analyzed the coherence between canal and afferent spontaneous activity (METHODS). At frequencies near $f_e = f_c$, we observed high levels of coherence (Fig. 4, asterisk), $\leq$0.8. This supports our model in which the f_e peak is attributed to periodic forcing of afferent firing by the canal oscillations, by way of the hair cell-to-afferent synapses.

Close examination of Fig. 4 (*bold trace*) reveals that the peak in the coherence was shifted to a frequency slightly less than $f_e = f_c$. A frequency shift is expected when a population of oscillators (e.g., in the different canals of the receptive field) each provides partial coherence (Bendat and Piersol 2000). In some recordings, afferent-canal coherence near f_e was not present or was small ($<$0.1), probably because of synaptic input to the afferent from other canals (as many as 30) in the receptive field, whose activities are statistically independent and so act as background noise. This interference was circumvented in experiments of inactivating all but one canal, removing the interference from other canals: then the coherence was $\approx$1 between afferent firing and the oscillations in the single canal remaining viable, precisely at $f_e = f_c$ (Russell and Neiman, unpublished data).

In control studies, the coherence was flat, near zero, when calculated between an afferent's firing and the oscillations of a canal outside its receptive field (Fig. 4, *gray skyline trace*). As a computational control, a surrogate times series was generated for the canal signal of Fig. 4, using the software package TISEAN (Hegger et al. 1999), which uses the amplitude-adjusted Fourier transform method proposed by Theiler et al. (1992) and modified by Schreiber and Schmitz (1996) to produce surrogates that preserve the power spectrum of data but randomize its phase information. The surrogate canal signal had a power spectrum identical to that of Fig. 4, *canal PS trace* (not illustrated). However, randomizing the phase destroyed any coherence between the canal and afferent (Fig. 4, *thin black trace*): all peaks were eliminated, leaving only small baseline fluctuations. This confirms that the coherence peak near $f_e = f_c$ in Fig. 4 (asterisk) arises from correlations between afferent and canal activity at this frequency.

Variable and invariant features of afferent power spectra. To try to estimate the "true" form of afferent power spectra, data from different afferents were compared, limiting the data set to files collected early from healthy fish, all at similar temperatures (21.8 $\pm$ 0.6°C), given that ER epithelial oscillations and also afferent firing are known to be temperature-sensitive (Braun et al. 1994; Lu and Fishman 1995). In the examples of Fig. 5*A*, the f_e peaks were all similar in frequency, about 26 Hz, whereas the f_a peaks ranged from 44 to 64 Hz. That is, the f_e peak was consistent in frequency for different electroreceptors, even in different fish, whereas the f_a frequency could vary 2-fold between different electroreceptors, even in the same fish (all at fixed temperature). In a sample of 22 afferents meeting the above criteria (from 11 fish), f_e =

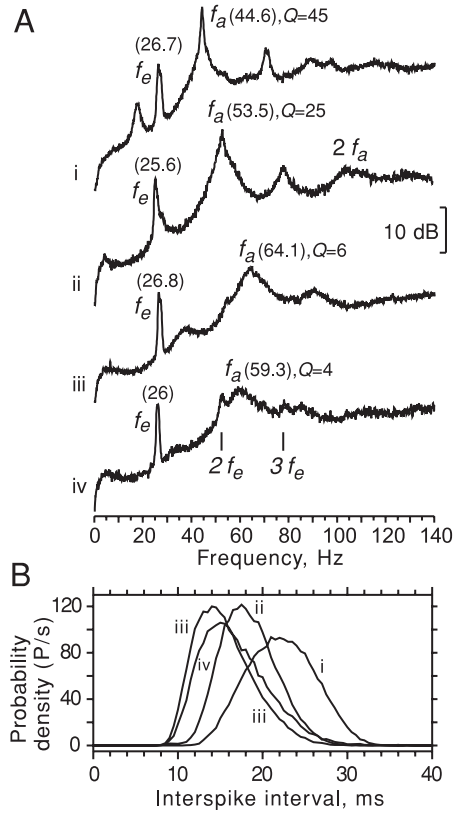

FIG. 5. Variants of afferent power spectra. *A*: logarithmic spectra for spontaneous firing of 4 different afferents, each from a different fish, all $<$6 h old. f_a, peak attributed to afferent oscillator. f_e, peak attributed to epithelial oscillators. Frequency values are in parentheses. Quality factors (Q) of the f_a peaks are listed. Temperatures were 21.7–22.4°C. *B*: ISI histograms for same data as *A*, with corresponding labels *i–iv*. Bin width = 0.5 ms. Areas under the 4 curves are equal. *Trace iv* had a long tail continuing out to 50 ms.

Downloaded from jn.physiology.org on June 27, 2007

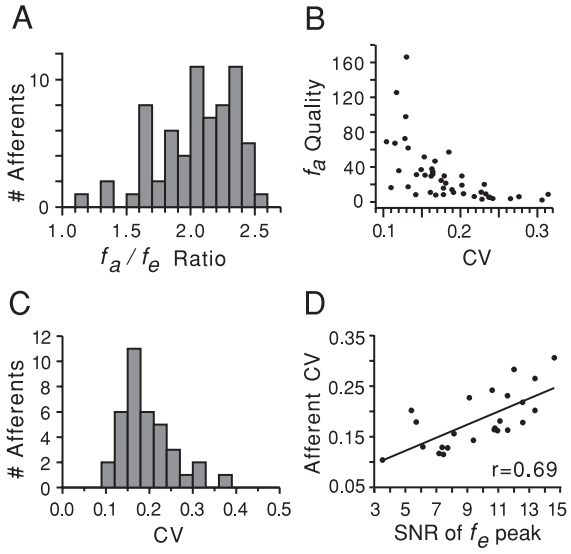

FIG. 6. Relations of power spectral peaks to other metrics of spontaneous afferent firing. *A*: histogram of ratios of the f_a frequency to the f_e frequency, from power spectra for 67 afferents. *B*: inverse relation between the coefficient of variation (CV) of afferent firing and the quality factor Q of the f_a peak in afferent power spectra; same afferents as *A*. *C*: unimodal histogram of CV values, for 37 afferents with mean firing rates of 45–69 Hz, at 21.2–23.4°C. *D*: direct relation between the CV of afferent firing and the signal-to-noise ratio (SNR) of the f_e peak in afferent power spectra, calculated as in Fig. 3*B*, as evidence that epithelial oscillations act as internal noise; data from 24 afferents at 22.1 ± 0.6°C. *r*, correlation coefficient.

25.4 ± 1.3 Hz (range 22.6–27.3 Hz) and f_a = 52.9 ± 9.5 Hz (range 27.8–67 Hz), giving coefficients of variation of 0.053 for f_e compared with 0.180 for f_a, again illustrating that the afferent frequency was more variable.

Different afferents varied widely in the height and width of the f_a peak. For example, in Fig. 5*Ai* the f_a peak was narrow and high, whereas in Fig. 5*Aiv* it was relatively broad. In a few afferents, the broad f_a peak was actually lower than the f_e peak. Even when a pair of afferents was recorded simultaneously, with the water flow stopped, both the narrow and broad types of f_a peaks were observed (not illustrated). We have no reason to choose any one of the spectra in Fig. 5*A* as best representing the "normal" activity of afferents, which rather tends to vary.

The different shapes of the f_a peak in Fig. 5*A* corresponded to different types of ISI histograms. High-power narrow f_a peaks corresponded to symmetrical narrow distributions (Fig. 5*Bi*), whereas low-power broad f_a peaks corresponded to wide highly skewed gamma-like distributions (Fig. 5*Biv*). ISI histograms contain the same information as in shuffled surrogates (see, e.g., Plesser and Geisel 2001), and so are not capable of revealing correlations between spikes, such as arise from the oscillatory input to afferents from canals.

Quantitative relations of afferent power spectral peaks. 1) The ratio of the f_a and f_e frequencies (f_a/f_e) was 2.05 ± 0.31 (range 1.15–2.52, for n = 67 afferents from 19 fish). That is, the f_a oscillator ran at about twice the f_e frequency. Nevertheless, the 2 oscillators were almost never locked in a rational (integer) relationship of exactly 2, as can be seen from a histogram of the ratio values (Fig. 6*A*), which is skewed toward ratios >2, peaking at ratios of 2.3–2.4. *2*) The quality factor of the f_a peak was inversely related to the coefficient of variation (CV) of ISIs (Fig. 6*B*). That is, high-power narrow f_a peaks corresponded to less variable firing. *3*) CV values for different afferents were unimodally distributed (Fig. 6*C*). This differs from the bimodal distribution observed for vestibular afferents (Goldberg and Fernandez 1971), consistent with the lack of calyx synapses in paddlefish ERs (Jørgensen et al. 1972). *4*) We hypothesize that the canal oscillations act as a source of internal noise and are responsible for part of the variability of spontaneous afferent firing. Evidence for this came from comparing the CV of spontaneous afferent firing to the SNR of the f_e peak in afferent power spectra. That is, the SNR of the f_e peak was used as a measure of the "strength" of canal oscillation input to an afferent. The SNR was calculated as in Fig. 3*B*, using shuffled surrogates to define the baseline level. As Fig. 6*D* shows, there was a tendency to develop higher CV values as the SNR of the f_e peak increased. That only a partial correlation (coefficient = 0.69) was observed suggests that there are other sources of variability in afferent firing, besides the canal oscillations. Data from afferents with low-frequency (1–10 Hz) spectral peaks attributed to water motion were excluded because water motion also strongly affected afferent firing, acting as external noise, yielding artifactually low-Q shapes of f_a peaks.

PHASE ANGLE MAPS DEMONSTRATE TWO TYPES OF OSCILLATORS. We used an alternate approach from nonlinear dynamics, phase angle maps (see METHODS), to confirm that the spontaneous firing patterns of ERs show 2 fundamental frequencies (i.e., show biperiodicity). A phase angle map for an ER afferent (Fig. 7) clearly demonstrated 2 lines, a topology that is characteristic for quasiperiodic (biperiodic) oscillations (Glass and Mackey 1988; Janson et al. 2001). Blurring of the lines was attributed to noise. This proves that the background firing pattern of ERs is biperiodic, by an independent approach that does not rely on correlation analyses. It also proves that the 2 frequencies need not form exact integer ratios, just as we observed for the canal (f_c) and afferent (f_a) oscillator frequencies. The f_a/f_c ratio was 2.5 in Fig. 7, consistent with little tendency toward fixed points. In other data, phase angle maps showed similar lines when the flow of ventilatory water was stopped (not illustrated).

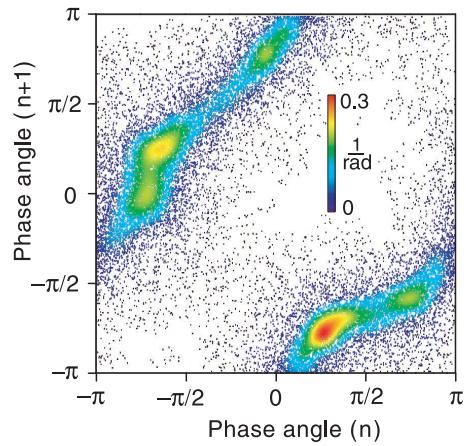

FIG. 7. Maps of phase angles (ϕ), between 25,032 sequential ISIs. Double lines (attractor) in each map demonstrate biperiodicity (see text). For either axis, the probability density of points is color coded; scale units = 1/radians (rad).

Downloaded from jn.physiology.org on June 27, 2007

Different responses of the two types of oscillators to external perturbations

EXTERNAL ELECTRICAL STIMULATION. Our aim was not to characterize the responses or sensitivity of paddlefish ERs per se, but rather to demonstrate that the epithelial and afferent oscillators respond differently to perturbations. Electrical stimuli were presented as voltage gradients in the water around the rostrum, applied between plate electrodes at the ends of the experimental chamber, or applied from a local dipole placed over the receptive field of an afferent. The ampullae of Lorenzini of cartilaginous fishes respond best at 1–10 Hz, and are excited by cathodal stimuli (i.e., when an electrode near the skin pore is made negative, relative to the environmental water), and inhibited by anodal stimuli; paddlefish ERs conform to this description (Pei et al. 1998; Wilkens et al. 1997).

Noise. When computer-generated Gaussian wideband noise was applied, the firing pattern of afferents changed qualitatively, to a bursting mode (Fig. 8*A*, *afferent trace*; Neiman and Russell 2002). The bursts occurred at irregular intervals and had variable durations (i.e., were stochastic). The firing rate during a burst followed a parabolic time course, rising to a maximum and then declining, and could achieve peak firing rates ≤250 Hz. Bursting became more pronounced as the noise amplitude was increased, seen as increased height of a short-latency peak in autocorrelograms of afferent firing (e.g., at 5–10 ms), attributed to fast intraburst firing (not illustrated; see Gabbiani and Koch 1998). In contrast, the oscillatory activity of canals was scarcely changed during noise stimulation (Fig. 8*A*, *canal trace*). The frequency of canal oscillations remained similar over a wide range of noise amplitudes, and there was little effect on the quality factor of the fundamental (f_c) peak in power spectra of canal oscillations. However, the canal oscillations could stop briefly after cessation of high-amplitude noise.

That external stimulation affected the afferent firing without altering the canal oscillations is seen in the afferent power spectra of Fig. 8*B*. Compared with the spectrum for spontaneous activity (Fig. 8*B1*), stimulation with increasing amplitudes of noise (Fig. 8, *B3* and *B4*) progressively broadened and diminished the f_a peak, as expected for noise effects on an oscillator, whereas the f_e peak persisted and did not become broader, consistent with the stimulus not affecting the canal oscillations.

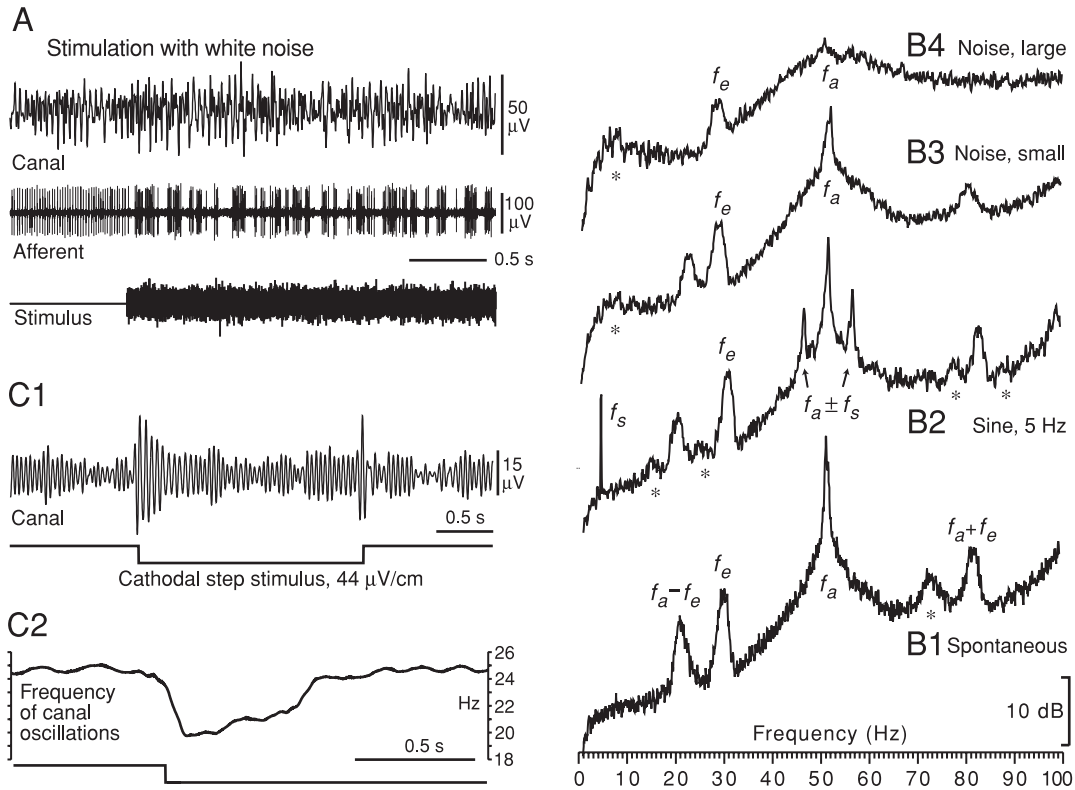

FIG. 8. Effects of electric field stimulation on oscillators. *A*: responses of canal oscillations and afferent firing to computer-generated white noise applied between plate electrodes, 223 μV/cm r.m.s. amplitude. Noise had little effect on canal oscillations, but evoked bursting of this single-unit afferent. The stimulus was cancelled out of the canal trace by differential recording. *B*: logarithmic power spectra of afferent firing during external stimulation, all from the same afferent. *B1*: control spectrum during background firing. f_a, peak attributed to afferent oscillator. f_e, peak attributed to epithelial oscillators. $f_a \pm f_e$, sideband peaks at combination frequencies. Asterisk: sideband peak at frequency $2f_a - f_e$. *B2*: spectrum during weak 5-Hz sine wave stimulation between plate electrodes, at 1.65 μV/cm p-p amplitude. f_s, spectral line at stimulus frequency. Asterisks: minor peaks at $f_a \pm f_e \pm f_s$ attributed to splitting of sideband peaks. *B*: *3* and *4*: spectra during stimulation with noise from an electronic generator, at 2.2 μV/cm r.m.s. amplitude (*B3*) or 5.5 μV/cm (*B4*). *Asterisk*: broad low-frequency peak attributed to stochastic bursting. *C*: effects of square-wave step stimuli on canal oscillations. *C1*: cathodal 2-s step between plate electrodes, of high-amplitude (44 μV/cm). The canal recording was digitally low-pass filtered at 35 Hz to show only the fundamental oscillation frequency. *C2*: transient fall in the frequency of canal oscillations at the start of a 44 μV/cm cathodal step stimulus. Instantaneous frequency of canal oscillations was measured from zero-crossings after low-pass filtering at 35 Hz, smoothed over a 0.1-s moving window, and averaged over 28 trials. The change in frequency appears to start before the stimulus because of the moving integration time.

Downloaded from jn.physiology.org on June 27, 2007

Sine waves. When a weak sine wave stimulus (about 3× threshold) was applied, only the f_a peak was affected, which split to show sidebands at $f_a \pm f_s$, where f_s was the stimulus frequency (Fig. 8*B2*). The $f_a \pm f_e$ combination peaks were also split to develop sidebands at frequencies $f_a \pm f_e \pm f_s$ (asterisks), suggesting that the combination peaks may provide additional frequency bands for encoding stimulus information. In contrast, the f_e peak associated with canal oscillations was unaffected by sine wave stimuli. Its amplitude and frequency did not change, and it did not develop discernible sidebands at $f_e \pm f_s$. Thus sine wave stimulation affected only the afferent oscillator, not the canal oscillations.

Steps. As noted by Clusin and Bennett (1979a), canal oscillations transiently become larger in amplitude at the onset of cathodal (excitatory) step stimuli, and smaller at the onset of anodal (inhibitory) steps, as we document here for paddlefish receptors (Fig. 8*C1*). Although weak- to intermediate-amplitude stimuli had little effect on the frequency or phase of canal oscillations, some effects were detected at the onset of high-amplitude cathodal step stimuli, detected by averaging the instantaneous frequency of canal oscillations over several trials. This revealed a transient fall in frequency at the step onset, from about 25 to about 21 Hz in Fig. 8*C2*. The decline in frequency decayed with a time constant of about 0.5 s, and thus would not be noticed during higher-frequency stimulation. No such changes in the frequency of canal oscillations were observed during large *spontaneous* changes in amplitude: instead, their frequency could remain constant, or could switch to 2× or 3× harmonics of the fundamental frequency (Fig. 1, *B* and *C*).

THERMAL STIMULATION. Electroreceptors are known to be temperature-sensitive (Braun et al. 1994; Hensel 1974; Lu and Fishman 1995; Sand 1938). Changing the temperature at ERs was an alternate way to perturb them, leading to different responses of the afferent and canal oscillations, as evidence that they are distinct processes. In response to a long step change in temperature, the static firing rate of paddlefish ERs (labeled "3" in Fig. 9*A*) became faster during warming, and slowed during cooling. However, for a brief time just after a step in temperature, the afferent firing rate did the opposite (labeled "2" and "4" in Fig. 9), attributable to thermoelectric properties of the gel in the canals (Brown 2003). Here, we are concerned with only the static response.

Different static temperature dependency of oscillation frequencies. The frequency of the afferent and canal oscillators had different temperature sensitivities, as calculated from the f_a and f_e peaks in power spectra of spontaneous firing near the end of temperature shifts lasting 100–300 s, long enough to approach steady state at the new temperature. In some cases, the activity of a canal in the receptive field was also recorded and f_c calculated.

The static temperature sensitivity of the frequency of canal oscillations (f_c or f_e values) was about 1.5 Hz/°C near 22°C. Data from 54 different canals or afferents could be fit with the power relation $f_{c,e} = -3.7 + 9.2 \times 10^{0.023T}$ Hz, with $r = 0.95$ (circles and line 3 in Fig. 9*B*, including one ER tested over a wide range of temperatures, open circles). This power relation has a slope of 1.5 Hz/°C at 22°C and corresponds to a Q_{10} of 1.8. Figure 9*B* indicates that the frequency of canal oscillations should exceed that of afferent firing at temperatures <10°C, where lines 1 and 3 cross, and this was observed in some paired recordings.

In contrast, the static temperature sensitivity of the f_a frequency, or afferent oscillator, was 2- to 3-fold larger, about

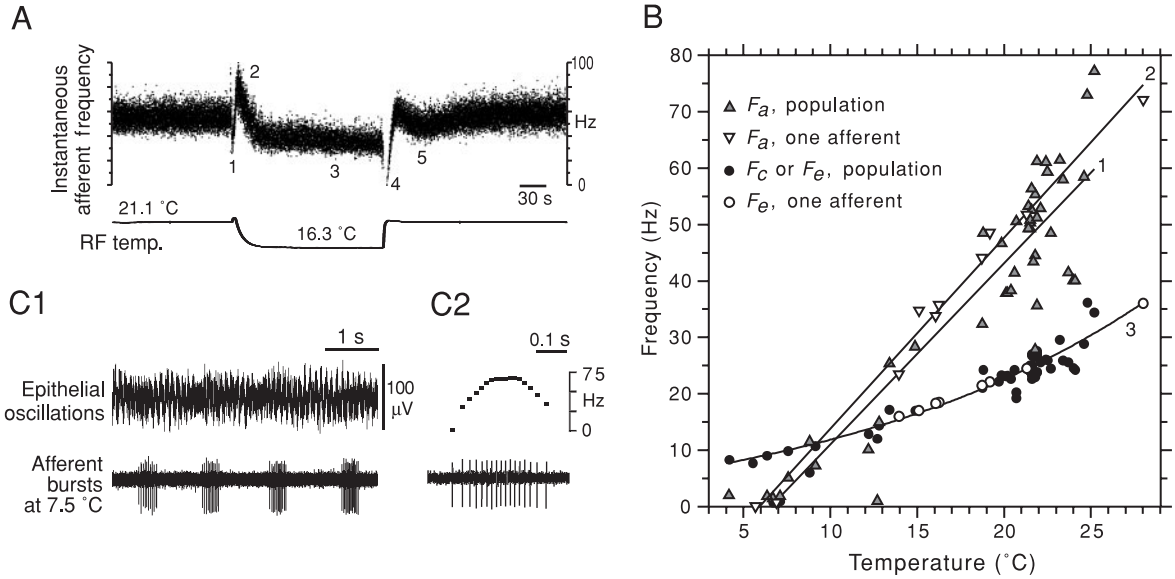

FIG. 9. Temperature effects on the frequency of spontaneous afferent firing and canal oscillations. *A*: time course of changes in the instantaneous frequency of an afferent's firing while streaming cold water focally onto the receptive field (RF); a latching solenoid valve was used to switch between an approximately 22°C source of water (start, end) and water chilled to 16.3°C, whose temperature (temp.) was monitored near the RF skin. Numbers identify parts of the response time course (see text). *1*: brief transient attributed to pulsation when switching the valve. *5*: adaptation. *B*: temperature effects on the steady-state fundamental frequency of afferent (f_a, triangles) or epithelial (f_c or f_e, circles) peaks in power spectra of background activity. For line *3*, 3 outlying points at low temperatures were excluded. *C1*: spontaneous bursting of an afferent (*bottom trace*) whose receptive field was chilled to 7.5°C using a focal stream of chilled water. Simultaneous recording from a canal in its receptive field (*top trace*) was a control to show that there was no epithelial activity correlated with the afferent bursts, just typical canal oscillations at 9.8 Hz. *C2*: parabolic time course of afferent firing frequency during a burst.

Downloaded from jn.physiology.org on June 27, 2007

3.2–3.4 Hz/°C. It could be represented by the line $f_a = 3.2T - 20$ Hz, with a correlation coefficient $r = 0.92$ (gray triangles and line 1 in Fig. 9*B*, for 40 different afferents from 13 fish). Data for one afferent tested over a wide range of temperatures gave similar results, $f_a = 3.4T - 20$ Hz (white inverted triangles and line 2 in Fig. 9*B*; $r = 0.99$). A linear relation gave a better fit than a power relation because the latter failed badly below 13°C, attributed to the afferents firing more slowly than predicted. The observed temperature sensitivity of about 3.2–3.4 Hz/°C probably overestimates the specific (intrinsic) thermal sensitivity of the f_a oscillator, given that the temperature of water flowing onto a receptive field will also exert indirect effects on an afferent resulting from thermal changes in its synaptic excitation by hair cells. The different thermal sensitivities of the $f_{e,c}$ and f_a frequencies support our hypothesis that they represent distinct oscillators.

Afferent bursting at low temperature. We observed spontaneous repetitive bursting of some afferents when their receptive field was chilled to 7–10°C with a focal stream of cold water, indicative of oscillatory processes. The afferent bursting could occur while there were no noticeable changes in canal oscillatory activity (Fig. 9*C1*), indicating that bursting arises in the afferent terminal. The firing rate during bursts followed a "parabolic" time course (Fig. 9*C2*). The temperature range at which we observed spontaneous bursting, 7–10°C, is within the range encountered by paddlefish in winter (Rosen and Hales 1981). Paddlefish stop feeding twice during the year, during summer (July–August) and also winter (January–March) (Rosen and Hales 1981). This has been attributed to food scarcity, but an alternate hypothesis is that electroreceptors, their primary means of locating prey, may be nonfunctional at these times because of extremes of water temperature.

Different time courses of temperature effects. Additional evidence that the $f_{e,c}$ and f_a oscillators are distinct came from their different behaviors during step shifts in temperature. The frequency of canal oscillations always promptly tracked the change in water temperature, measured at the skin using a miniature sensor. For example, in Fig. 10*A*, the f_e peak stepped up promptly from 24 Hz at 21.8°C to a maximum of 36.3 Hz during focal warming of the receptive field to 28.1°C. There was little adaptation: f_e declined only 8% by the end of this 300-s application of warm water.

In paired recordings, the time course of the f_c peak from canal recordings was similar to the time course of the f_e peak from afferent power spectra (Fig. 10*B*). The 2nd, 3rd, and so forth harmonics of f_c showed temperature shifts that were 2×, 3×, and so forth larger than that of f_c (Fig. 10*B*, *bottom panel*), such that their temperature sensitivities were multiples of that for f_c.

In contrast, the frequency of the afferent oscillator showed marked adaptation and delay. For example, after the onset of warming in Fig. 10*A*, the frequency of the f_a peak increased slowly from 55.8 Hz to a maximum of 90.1 Hz, reached after a delay of 84 s. The f_a frequency then adapted, declining eventually to 71.4 Hz, losing 55% of the initial increase. That is, it went through a delayed peak even though the skin was still being warmed (*temperature sensor trace*), and followed a

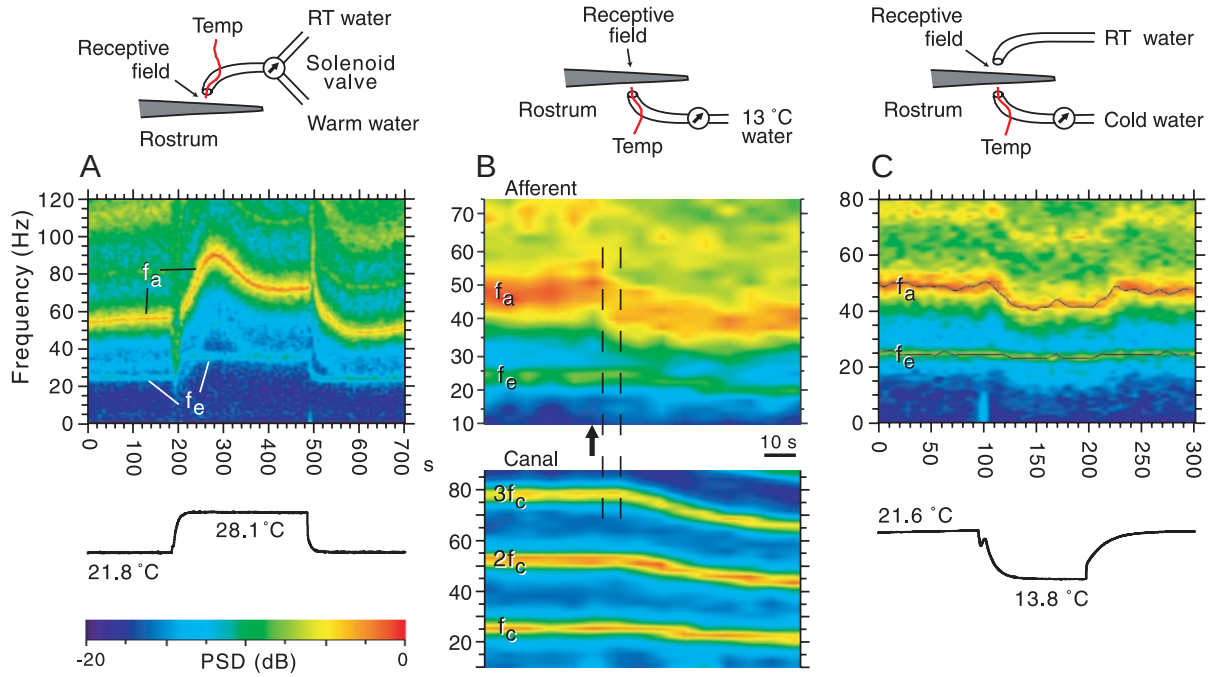

FIG. 10. Thermal gradients demonstrate separate locations of the 2 types of oscillators. *Top panels*: experimental designs for *A*, *B*, and *C* are shown as schematics. Gray: cross section of one side (half) of the rostrum. Temp, temperature sensor, whose output is shown in *bottom panels*. Arrows: valves. *Center panels*: power spectra of afferent firing, with logarithmic power spectral density coded as color (scale, *bottom left*). *A*: warming step lasting 300 s. f_a, peak attributed to afferent oscillator. f_e, peak attributed to epithelial oscillators. *B*: after the onset (arrow) of cooling underneath the receptive field, the afferent oscillator started changing frequency about 6 s before the epithelial oscillators (vertical dashed lines). Frequency of canal oscillations, recorded directly, was monitored from the 3rd harmonic of their fundamental frequency ($3f_c$) in a logarithmic power spectrum (*bottom panel*). *C*: depths below the skin of the afferent and epithelial oscillators were measured using a thermal gradient created by continuously flowing 22°C water onto the dorsal receptive field, while switching ON-OFF another stream of cold water onto the ventral surface of the rostrum, underneath the receptive field. Lines were fitted to maxima of the f_e and f_a traces.

Downloaded from jn.physiology.org on June 27, 2007

very different time course than the f_e peak, as evidence for distinct oscillatory processes.

Localizing the oscillators using thermal gradients. We took advantage of the planar geometry of the rostrum, which is wide and flat but relatively thin, to create thermal gradients through the rostrum, between its dorsal and ventral surfaces (see METHODS). This made it feasible to test whether the canal and afferent oscillators were *spatially separate*, because if they were at different depths below the skin they would experience different temperatures during the application of a vertical thermal gradient. We used dorsal receptive fields located near midlength on the rostrum, and about halfway between edge and midline, where the rostrum was about 2.5 mm thick. A cross section of one side of the rostrum is shaped like a triangle, tapering from about 5 mm maximum thickness at the midline to about 1 mm at the edge (*schematics*, Fig. 10).

There were different latencies of shifts in the f_a and f_e peaks, after the application of a thermal gradient. For example, in Fig. 10*B*, the ventral surface of the rostrum was chilled while recording afferent firing along with canal activity of a dorsal ER; water flow started at the arrow. This was intended to set up a thermal gradient in a vertical column of tissue encompassing the receptive field. The f_a peak began changing frequency about 6 s before any change in the canal f_c frequency, indicating that the f_a oscillator was located deeper below the dorsal surface than the f_c oscillator. We monitored changes in the canal oscillator frequency from its 3rd harmonic (Fig. 10*B*, *trace 3f_c*, *bottom panel*), which has a thermal sensitivity of about 4 Hz/°C, similar to that of the f_a peak.

A critical experiment was to clamp the receptive field skin near ambient temperature using a continuous flow of about 22°C water onto the dorsal surface, while switching on or off a flow of cold water onto the ventral surface underneath the receptive field, thereby creating a thermal gradient through the tissue. In the example of Fig. 10*C*, the receptive field received 21.6°C water, while 13.8°C water was applied underneath. The frequency of the epithelial oscillations (f_e) changed little when the ventral surface was cooled, declining from 24.6 to 23.4 Hz ($\Delta f = -1.2$ Hz). Assuming a value of 1.5 Hz/°C for the specific thermal sensitivity of canal oscillations (near 22°C, above), the f_e oscillator experienced a temperature change of -1.2°C/1.5 Hz/°C $= -0.8$°C. If the temperature gradient is assumed to be linear, for a rostrum thickness of 2.5 mm, then the depth of the f_e oscillators below the receptive field skin can be calculated as 0.8°C/3.12°C/mm = 0.25 mm in this example, or 0.27 ± 0.02 mm for 4 trials in 2 fish.

The afferent oscillator was located deeper below the skin, calculated as follows: The frequency of the f_a peak declined from 47.7 to 41.0 Hz during the flow of cold water in Fig. 10*C* ($\Delta f = -6.7$ Hz). Using a value of 3.4 Hz/°C for the temperature sensitivity of the f_a peak, the depth of the afferent oscillator below the receptive field skin was calculated as 0.63 mm for the example of Fig. 10*C*, or 0.53 ± 0.14 mm for 5 trials on 3 afferents in 2 fish. Calculating the depth of the f_a oscillator depends on knowing its *specific* thermal sensitivity; the observed value of 3.2–3.4 Hz/°C from Fig. 9*B* is probably an overestimate, as explained above. If a lower value is assumed for the specific thermal sensitivity of f_a, then the calculated depth of the f_a oscillator would be even greater. An analogous approach was used by Hensel and Zotterman (1951).

In related experiments, we completely separated the behavior of the afferent and epithelial oscillators by heating slightly the water flowing onto the skin, while chilling underneath the receptive field, such that there was no measurable change in the f_e frequency, whereas the f_a oscillator still showed large changes in frequency.

These experimental data support our hypothesis that there are 2 distinct types of oscillators embedded into the structure of paddlefish electroreceptors, with separate locations. The calculated depth of the f_e oscillator correspond well to the morphological depth of the sensory epithelia, at the internal end of canals about 0.25 mm in length (Jørgensen et al. 1972). The deeper calculated depth of the f_a oscillator corresponds to the location underneath a cluster of canals where 2–5 afferent axons in a small nerve divide into branches to innervate all the canals of the cluster, as seen in DiI-labeled preparations (not illustrated). However, we do not yet know where spikes are initiated in these afferents, or whether spikes are initiated at only a single site per afferent (Chimento and Ross 1996). The data suggest that spikes are probably not initiated at the synaptic contacts from hair cells because this would predict that the f_e and f_a oscillators would have similar depths below the skin. Our data cannot exclude some lateral displacement of the f_a oscillator, given that a thermal gradient affected a vertical column of tissue >4 mm in diameter, whereas receptive fields are ≤1 mm in diameter.

Functional relations between canal and afferent oscillations

EXTENDED ANTICORRELATIONS OF INTERSPIKE INTERVALS ARISE FROM BIPERIODICITY A functional consequence of having 2 different oscillatory processes in paddlefish ERs is the creation of long-lasting ("extended") correlations between sequential ISIs, extending over 20–40 or more ISIs, corresponding to a few hundred milliseconds. Here, we demonstrate that the afferent spiking represents a nonrenewal point process, that groups of 20–40 afferent spikes have internal structure in their spike timing, a type of "memory," and that this depends on the epithelial and afferent oscillations. Anticorrelations between spike intervals can enhance receptor sensitivity by reducing higher-order variability (Chacron et al. 2001; Ratnam and Nelson 2000).

Return maps (see METHODS) showed that a short ISI tended to be followed by a long ISI, and vice versa, such that a plot of each interval T_n against the subsequent interval T_{n+1} followed an approximately inverse relation (Fig. 11*A*). A histogram of the ISIs is included to emphasize that the anticorrelated fluctuations occurred over the normal range of ISIs (Schäfer et al. 1995). However, low values near the line $T_{n+1} = T_n$ were more common than expected from an inverse relation. The data in Fig. 11*A* were collected while the flow of ventilatory water was stopped, so water flow noise was absent. Such pairwise anticorrelations of sequential ISIs have been observed for other auditory and ER afferents (Braun et al. 1994; Chacron et al. 2001; Lowen and Teich 1992; Ratnam and Nelson 2000; Schäfer et al. 1995).

The serial correlation coefficient $C(k)$ (see METHODS; Tuckwell 1988), reveals the duration and dynamics of correlations between spike intervals because it gives the *average* autocorrelation as a function of the ISI number k after an interval T_0 being considered. Figure 11*B* shows that after a spike, the length of the following average ISIs tended to alternate in sign,

Downloaded from jn.physiology.org on June 27, 2007

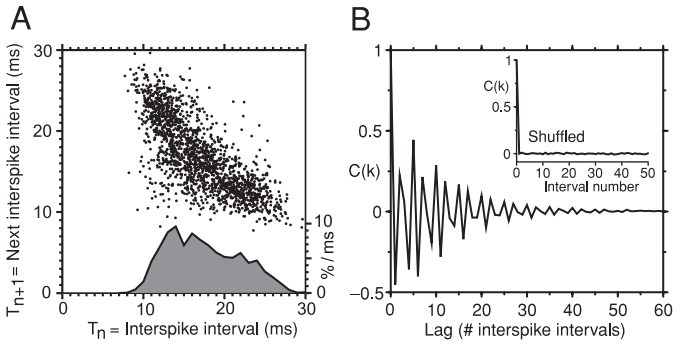

FIG. 11. Anticorrelations of sequential ISIs. *A*: return map for 1,936 sequential pairs of ISIs, T_n and T_{n+1}, from 30 s of background afferent firing shortly after stopping the flow of ventilatory water. Also shown is the ISI histogram, expressed as the % of ISIs per 1-ms bin (right-side vertical axis; summed area under curve = 100%). *B*: extended anticorrelations of ISIs during spontaneous firing. *k*, lag after a given ISI, expressed as the number of elapsed ISIs. *C*(*k*), serial correlation coefficient. *Inset*: surrogate control; serial correlation coefficient for the same data after repeatedly shuffling the order of ISIs.

between being opposite or similar in their deviation from the mean interval $\bar{T}$. Hence $C(k)$ assumed a negative (anticorrelated) value for $k = 1$, a positive (correlated) value for $k = 2$, and usually alternated thereafter. The magnitude of such anticorrelations decayed progressively, reaching baseline (insignificance) by 20–40 ISIs, equivalent to 300–900 ms, depending on the mean firing rate. Their exponential decay was characterized by the correlation length k_c, the number of ISIs for $C(k)$ to decay to $1/e$, which was 5.9 ± 1.9 intervals, equivalent to 90–130 ms, for the spontaneous firing of 25 afferents.

Evidence that extended anticorrelations result from the biperiodic organization of ERs includes the following: *1*) The time course of the decay depended on the ratio of the f_a and f_e frequencies. The anticorrelations were exaggerated and decayed slowly in afferents with $f_a \approx 2f_e$, but were briefer and smaller if f_a departed far away from $2f_e$ (not illustrated). *2*) Sometimes pronounced waxing and waning (beating) of the anticorrelations was observed (not illustrated), as expected for a quasiperiodic regime in a system of 2 coupled oscillators. The beating was most marked if f_a was close to $2f_e$. Such beating would not be expected from alternative models of a single oscillator that was period-doubled (Anishchenko et al. 2002). *3*) The firing of afferents in aged fish preparations, in which the canal oscillations had disappeared along with the f_e peak in afferent power spectra, did not show extended anticorrelations (Neiman and Russell 2001).

As a computational control, the anticorrelations were destroyed when the order of ISIs was shuffled repeatedly to form a renewal stochastic process (Fig. 11*B*, *inset*) (Lowen and Teich 1992), consistent with the shuffling removing from an afferent's power spectrum the peaks associated with epithelial oscillations.

REVERSE CORRELATION OF AFFERENT SPIKES TO CANAL OSCILLATIONS. Reverse correlation (revcor; see METHODS) between an afferent's spikes and a canal signal revealed an attenuated afferent spike near the center of a packet of slow waves (Fig. 12*A*), near the negative-to-positive zero crossing of a slow wave. The packet of canal oscillations grew in amplitude over a few hundred milliseconds preceding a spike, reached a maximum amplitude near the spike, and decayed after it. The frequency inside a wave packet was similar to f_c, but slightly lower. For example, in Fig. 12*A*, the frequency of waves in the packet was 19.4 Hz, whereas the mean frequency of raw canal oscillations was 21.2 Hz. The decay time for the amplitude of the revcor packet to decline to $1/e$ of maximum was about 165 ms for this canal at 20.7°C. At higher temperatures, the packets were more prolonged and exaggerated. These revcor data show that afferent firing is partly correlated with the oscillations in a given canal.

The attenuated spike usually had a positive-going polarity, showed a threshold-like inflection on the rising phase, sometimes was followed by an undershoot, and had an amplitude of 7.3 ± 3.4 μV. The conduction delay from the peak of a canal's attenuated spike to the peak of the ganglion spike (*inset*, Fig. 12*A*) ranged from 2.4 to 5 ms, and was longer for receptive fields near the rostrum tip. This delay was used to estimate conduction velocities of 33 ± 4 m/s, ranging from 27 to 42 m/s (for 9 afferents from 4 fish of 34–43 cm total length, at 20.7–21.9°C; the length of an afferent axon was estimated by laying a thread along the assumed axon path, based on dissections of nerves in the rostrum). Attenuated afferent spikes in canal signals gave rise to minor peaks in power spectra of canal signals (Fig. 2*A*, asterisk). The attenuated spikes probably arise by ephaptic coupling, attributed to the proximity of sensory epithelia to afferent terminals undergoing action potentials.

As a control, similar "pretriggered averaging" was carried out on signals from canals of adjacent clusters, not in the

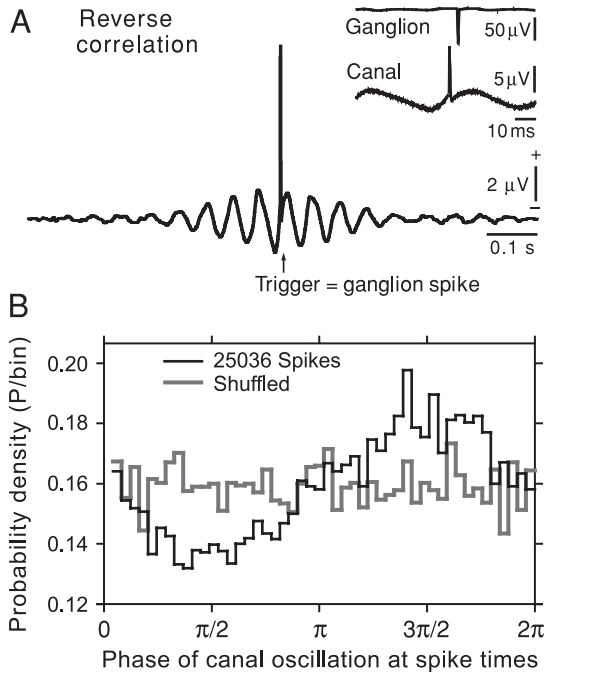

FIG. 12. Timing relations of afferent spikes to canal oscillations. *A*: reverse correlation, from pretriggered average of a canal's spontaneous signals, generated using afferent spikes recorded in the ALLn ganglion near the brain as the timing reference (*time 0*). Spikes tended to occur on the positive-slope phase of canal oscillations. The r.m.s. amplitude of spontaneous oscillations (nonaveraged) in this canal was 18.5 μV. *Inset*: attenuated afferent spikes in the canal signal (lower trace) preceded the soma spike (*top trace*) by 3.6 ms because of conduction time. *B*: average-phase histogram, showing the phase at which 25,036 afferent spikes occurred, relative to the cycle of canal oscillations, during a simultaneous recording of canal and afferent background activity. One cycle of canal oscillation is considered as 2π radians. The histogram has 50 bins, each 0.04π wide. *Black trace*: unshuffled data. *Gray trace*: surrogate control after repeatedly shuffling the order of ISIs.

Downloaded from jn.physiology.org on June 27, 2007

receptive field of the afferent under study: the revcor was essentially flat, with no spike at *time 0* (not illustrated). Hence a revcor waveform consisting of an attenuated afferent spike centered near the maximum of a spindle-shaped packet of slow oscillations can probably be used as a criterion for synaptic connection between a canal and afferent.

The revcor waveform in the time domain is mathematically related to the afferent-canal coherence in the frequency domain. Data that yielded a large-amplitude packet of oscillations in the revcor waveform also showed high coherence between afferent and canal at frequencies near $f_c = f_e$, and vice versa.

PREFERRED PHASE BETWEEN SPIKES AND CANAL OSCILLATIONS. Additional evidence for coupling of an afferent's firing to the oscillations of a given canal in the receptive field came from the probability distribution of their relative instantaneous phase φ_P (see METHODS). The example of Fig. 12*B* (*black trace*) showed a broad but well-expressed minimum at $\varphi_P = \pi/2$, and a maximum at $\varphi_P = 3\pi/2$, implying coupling of the afferent's firing to the canal's oscillations. This instantaneous phase distribution was significantly different from a uniform distribution ($P_{H_0} < 0.0001$, K-S test). By inspection, $\varphi_P = 3\pi/2$ corresponded to the zero crossing on the rising (positive slope) phase of the canal oscillations, agreeing well with our observations from revcor analysis. The minimum at $\varphi_P = \pi/2$ means that spikes occurred less frequently near the negative-slope zero crossing of canal oscillations. As a control, repeated shuffling of the order of ISIs gave an approximately flat phase distribution (Fig. 12*B*, *gray trace*), which was not significantly different from a uniform distribution ($P_{H_0} > 0.05$, K-S test), as expected for the relative phase of 2 oscillators that are not coupled.

Nevertheless, the 2 processes were not synchronized, in the strict sense of the word, which would instead predict narrow peaks at certain phases, and other characteristics such as entrainment (see Neiman et al. 2000). The broad maximum and minimum in Fig. 12*B* (*black trace*) merely point to average tendencies for spikes to occur, or not occur, at certain phases of a given canal's oscillations. Because there are 3–30 canals in the receptive field of an afferent, the afferent firing is probably not synchronized to any single canal's oscillations.

MISMATCH BETWEEN FREQUENCIES. A possible function of the canal oscillations could be to resonate with certain stimulus frequencies, thereby providing amplification and frequency selectivity, as has been proposed for the oscillations of cilia and membrane potential in auditory receptors of frogs (Camelet et al. 2000; Martin and Hudspeth 1999; Ospeck et al. 2001). To examine this, we mapped the frequency response of paddlefish ERs using stimulus reconstruction (see METHODS). This gave better frequency resolution than the use of discrete stimulus frequencies (Pei et al. 1998; Wilkens et al. 1997).

The maximal stimulus encoding by afferents occurred at about 5 Hz (upward arrow, Fig. 13), agreeing well with other reports. We would point out that the afferent frequency response declined precipitously in the range of stimulus frequencies near the 27-Hz frequency of canal oscillations (downward arrow, Fig. 13). In fact, there was notchlike reduction in the afferent frequency response precisely at the frequency of the canal oscillations, to nil, signifying little or no stimulus encoding. This notch was not revealed in previous measurements (Pei et al. 1998; Wilkens et al. 1997). Thus there is a severe

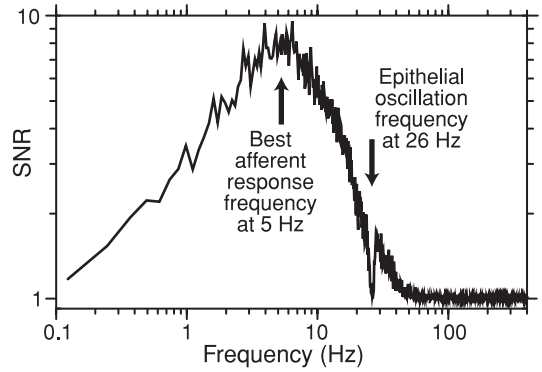

FIG. 13. Mismatch between the best stimulus frequency for driving an afferent's firing (upward arrow), and the frequency of canal oscillations in this afferent's receptive field (downward arrow), determined using a white noise stimulus reconstruction approach (see METHODS).

mismatch between the approximately 5-Hz frequency for best afferent response and the approximately 27-Hz frequency of canal oscillations, corresponding to 2–2.5 octaves. This mismatch makes it unlikely that the function of the canal oscillations in paddlefish ERs would be to mediate an amplification mechanism at corresponding stimulus frequencies.

DISCUSSION

Our analyses and experiments demonstrate that 2 distinct types of noisy oscillators are embedded into the structure of paddlefish electroreceptors. The receptor output is influenced by both types of oscillators and, as a result, is stochastically biperiodic (quasiperiodic), while also responding to external stimuli. Having 2 types of internal oscillators is a novel type of organization for a peripheral sensory receptor. Our findings illustrate that sensory receptors can be complex active systems rather than mere transducers of stimulus energy. Paddlefish ERs can be viewed as accessible peripheral "preprocessors," which substantially transform external electrosensory stimuli before sending output to the brain.

An experimental advantage of paddlefish ERs is that they permit simultaneous recordings of epithelial and afferent activity, something not achieved in other hair cell–primary afferent receptors of other modalities. Our use of in vivo preparations, with the cardiovascular system intact, and ventilation with oxygenated water, no doubt contributed to being able to observe the receptor oscillations, especially the epithelial oscillations, given that hair cell–primary afferent receptors are known to be susceptible to hypoxia (Manley 2001; Manley et al. 2001; Suzue et al. 1987).

Afferent oscillator

Evidence that each afferent terminal possesses a powerful 30- to 70-Hz oscillator, distinct from the canal oscillators, includes the following. *1*) The f_a peak in power spectra of afferent spike times has high power, can be narrow and sharp, and persists after shuffling ISIs, indicative of a basic periodicity of afferent firing. A random noisy process would instead predict a flat power spectrum, without sharp peaks. *2*) The center frequency of the f_a peak is identical to the mean firing rate, indicating a close relation to the afferent, where spikes are initiated. *3*) Bursting firing patterns can be evoked by noise

Downloaded from jn.physiology.org on June 27, 2007

stimulation (Neiman and Russell 2002), or low temperature, without corresponding canal activity. *4*) The afferent firing rate has temperature sensitivity different from that of the canal oscillations. *5*) Our thermal gradient experiments show that the f_a oscillator is located at a deeper tissue level than the canal oscillators, corresponding to the morphological location of afferent axons. *6*) External electrical stimuli strongly affect the f_a oscillator, but do not usually affect the canal oscillation frequency. *7*) Afferent spike timing can be synchronized by external periodic stimuli (Neiman et al. 2000), which happens only with oscillators.

Other types of sensory afferents contain an oscillator [e.g., mammalian cold receptors (INTRODUCTION)] that has been modeled as arising from 2 slow currents, driving spiking (Braun et al. 2000; Feudel et al. 2000).

Epithelial oscillators

The noisy voltage oscillations we have recorded from canals confirm the findings of Clusin and Bennett (1979a,b) and Lu and Fishman (1995). The pronounced peaks in power spectra of canal signals, at about 26 Hz and harmonics thereof, point to a strongly periodic process. Our thermal gradient experiments colocalized the oscillatory process with the sensory epithelia. Also, in the in vitro preparations we have developed of paddlefish ERs, we were able to remove the skin and canal from ERs using a vibratome, and then record similar oscillations using a small pipette aspirated directly onto a sensory epithelium, showing that the epithelium is the origin of the oscillations (Russell and Neiman, unpublished data); thus the term "epithelial oscillations" is justified.

The sensory epithelia of paddlefish ERs include an estimated 1,500 hair cells and many support cells (Jørgensen et al. 1972; Russell et al. 2003). The only previous evidence that the receptor cells (hair cells) undergo the oscillations was that corresponding oscillations could be recorded from tetrodotoxin-treated afferent nerves, occurring after a synaptic delay, in ampullae of Lorenzini (Clusin and Bennett 1979a). Because hair cells are the presynaptic element, their membrane potentials presumably oscillate (although this does not necessarily mean that the hair cells *generate* the epithelial oscillations). We provide additional evidence that the membrane potentials of hair cells oscillate, given that the f_e peak in afferent power spectra, which has identical frequency and high coherence to the canal oscillations, is driven synaptically.

The Gaussian distribution of canal signal samples, and the Rayleigh distribution of canal signal amplitudes, are consistent (ascribed to the central limit theorem) with canal oscillations arising as the summed activity of many independent generators. This is also suggested by the broadness of the f_c peak in canal power spectra ($Q_c = 17 \pm 4$, compared with the mean $Q_a = 31$ for the f_a peak in afferent spectra). We have modeled a sensory epithelium as a stochastic population of similar but nonidentical noncoupled van der Pol oscillators (Neiman and Russell 2001). The individual oscillators need to have nonidentical frequencies, ranging over a narrow distribution similar to what we report here, or else cancellation occurs in their summed activity. Clusin and Bennett (1979b) also invoked a population of noncoupled generators. Nevertheless, the possibility of coupling within an ER epithelium requires direct study. Gap junctions between hair cells and support cells have been reported in the vestibular sensory epithelia of certain vertebrates (Zahm 1980).

Coupling of epithelial and afferent oscillators

Ultrastructure shows that hair cells make chemical synapses onto afferent terminals in paddlefish ERs (Jørgensen et al. 1972), corresponding to unidirectional epithelia-to-afferent coupling. Nevertheless, the morphology, as well as the sidebands we observe in afferent power spectra, are consistent with 2 alternate models for the organization of paddlefish ERs: *1*) *Serial model*: The epithelial oscillators could be synaptic inputs to the afferent oscillator, which in turn drives a spike initiating zone. *2*) *Parallel model*: The f_e and f_a oscillators could be parallel inputs to a third element, a nonlinear mixer related to spiking (e.g., a threshold-dependent spike initiating zone). Any nonlinear mixer will produce sidebands when forced by 2 different periodic signals. The preferred phase relation that we observed between afferent spikes and canal oscillations is also consistent with either model. We consider the serial model to be more likely, based on experiments in which we varied the amplitude of epithelial oscillations, leading to changes in the frequency of the f_a oscillator (Neiman and Russell 2001; and unpublished).

Functional roles of receptor oscillators

The ERs of paddlefish are used for the vital behavior of feeding, and so it seems likely that their biperiodic organization represents an optimization. Its possible advantages could include the following.

1) The afferent oscillator provides a mechanism for driving spontaneous firing, conferring the advantage that both inhibitory and excitatory stimuli can be detected. By itself, the afferent firing would be nearly periodic, as we observe when the canal oscillations are absent (Neiman and Russell 2001). An alternate mechanism for driving spontaneous afferent firing, the continuous vesicular release of excitatory neurotransmitter from receptor cells, follows statistics different from those observed here (see Geisler 1998).

2) The afferent oscillator may provide a mechanism to deal with the huge synaptic convergence onto an afferent from $\leq$45,000 hair cells (e.g., in receptive fields of 30 epithelia, with an estimated 1,500 hair cells per epithelium). By having an afferent oscillator, the synaptic input from all the hair cells can modulate a single spike-generating process. It seems unlikely that each released vesicle of hair cell neurotransmitter would evoke an afferent spike, as posited for mammalian n.VIII afferents innervating only one or a few vestibular or auditory hair cells (Chimento and Ross 1996; Geisler 1998).

3) The epithelial oscillations definitely act as internal noise, evoking short-term variability in the spontaneous firing of afferents, increasing their CV. For example, the amplitude of canal oscillations correlates with the CV of afferent firing (Neiman and Russell 2001), as does the SNR of the f_e peak in afferent power spectra when different afferents are compared. Having a built-in source of appropriate-level noise may be advantageous in avoiding the vagaries of environmental (external) noise, improving receptor reliability. The epithelial oscillations resemble a special type of noise termed "harmonic noise" (i.e., noise having oscillatory components in a narrow

Downloaded from jn.physiology.org on June 27, 2007

frequency band) (Schimansky-Geier and Zülicke 1990). Examples of internal noise sources in other neural systems include the Brownian motion of cochlear fluid (Jaramillo and Wiesenfeld 1998) and ion channel noise in cortical neurons (White et al. 1998). An alternate mechanism for inducing irregular afferent firing is the stochastic vesicular release of transmitter (Geisler 1998; Goldberg et al. 1992; Teunis et al. 1991), which does not show periodicity.

4) The internal noise from epithelial oscillations may possibly mediate stochastic resonance (Douglass et al. 1993), to increase receptor sensitivity near threshold. Paddlefish ERs do show stochastic resonance in response to optimal-level external noise (Russell et al. 2001).

5) The internal noise from epithelial oscillations may serve to randomize the phase of spikes in different electroreceptors, to minimize inadvertent spike coincidences or phase locking, which could lead to false alarms during prey detection.

6) A definite consequence of the biperiodic organization is the induction of pronounced extended negative correlations between afferent spike intervals. The anticorrelations decay quasi-exponentially over several tens of intervals after a spike. We have shown experimentally that the ISI anticorrelations arise because of periodic forcing of the afferent oscillator by the epithelial oscillations, and disappear when the latter are absent (Neiman and Russell 2001). The ISI anticorrelations, and the peaks in afferent power spectra, which are absent in the corresponding shuffled (renewal) spike trains, make it clear that firing in paddlefish ERs is not a renewal process, that is, a point process in which every interspike interval is independent of all prior and subsequent intervals, as in shuffled surrogates (Tuckwell 1988). Instead, short sequences of afferent intervals are correlated, exhibiting "memory" that decays quasi-exponentially over 0.5–1 s after a spike. Anticorrelations of afferent ISIs can increase receptor sensitivity and discriminability, by reducing the higher-order randomness of spike time series (Chacron et al. 2001; Ratnam and Nelson 2000). For example, because long and short intervals tend to alternate, they compensate, such that variability is reduced when spike pairs are considered. Thus the noisy epithelial oscillations influence an afferent's firing in 2 disparate ways: On the one hand, they increase short-term variability, expressed as the CV. On the other hand, they increase order on longer time scales, by the extended anticorrelations of ISIs. Other examples of noise-enhanced order can be cited (Anishchenko et al. 1999). Lowen and Teich (1992) and Teich and Lowen (1994) reported that many mammalian auditory fibers show marked anticorrelations of sequential interspike intervals, firing in a nonrenewal process.

7) Having 2 types of internal oscillators expands the frequency and time scales available for the encoding of sensory information, given that external stimuli can modulate not only the f_a peak in afferent power spectra but also the sidebands at $f_a \pm f_e$.

8) If an electroreceptor, a biperiodic oscillator, is subjected to periodic external stimulation, a complex system with triperiodic motion results, and is expected to display a great variety of dynamical regimes. Multifrequency regimes are relevant to audition (Cartwright et al. 1999), cortical waves in the brain (Tass et al. 1998), heartbeat–respiration interactions (Schäfer et al. 1998), and other organ interactions (Glass 2001).

9) An alternative possibility is that the epithelial oscillations may drive secretion of gel from the support cells. The apical regions of support cells have many vesicles (Jørgensen et al. 1972), secreting the gel that fills the canal. Other secretory cells tend to be autoactive; epithelial oscillations may fulfill this role. This hypothesis would require that the support cells undergo 25-Hz membrane potential oscillations similar to the observed canal oscillations.

10) Another alternative possibility is that the water temperature could be encoded by frequency modulation of afferent firing. That is, the epithelial oscillations could act as a carrier wave whose frequency is a function of temperature, that periodically modulates an afferent's firing. This may in effect multiplex the afferent output to encode 2 different sensory modalities simultaneously.

Comparisons to other hair cell receptors

Auditory and vestibular hair cell receptors of vertebrates are known to undergo oscillations (see INTRODUCTION). Our findings may increase the understanding of basic vestibular and auditory mechanisms, given the homology assumed between cathodally excited ERs and the receptors of other n.VIII sensory systems (Gans 1992).

The frequency of spontaneous and evoked oscillations in turtle and frog auditory hair cells correlates well with the characteristic ("best") frequency of a given hair cell, as evidence that the oscillations contribute to frequency selectivity (Crawford and Fettiplace 1980; Fettiplace and Fuchs 1999; Martin et al. 2001). Another example is the tuberous type of ER, in which the frequency of oscillations recorded at a canal correlates well with the best frequency of a given receptor (Bullock 1982; Viancour 1979; Watson and Bastian 1979). However, the epithelial oscillations that we observe in paddlefish ERs do not conform to this model of a frequency-tuning mechanism because their frequency, at which there is near-zero encoding of external stimuli, is above most of the frequency response band of the receptors. This counterexample indicates that hair cell oscillations can have functional roles other than frequency selectivity.

Quasiperiodic firing patterns have been observed for auditory afferents of nonmammals. For example, the spontaneous firing of low-frequency afferents (having best frequencies in the 100- to 1,000-Hz band) may show "preferred intervals," whereby probability distributions of spontaneous ISIs show a series of discrete peaks at integer multiples of the modal interval (Crawford and Fettiplace 1980; Gummer 1991; Klinke et al. 1994; Köeppl 1997; Manley 1979; Temchin 1988). Preferred intervals arise from membrane potential oscillations in hair cells, along with "skipping" such that afferents do not fire on every hair cell cycle. Also, bursting has been observed for some goldfish and avian auditory afferents (Sento and Furukawa 1987; Temchin 1988), suggestive of an oscillator in certain afferents.

ACKNOWLEDGMENTS

We thank S. Bahar, H. Braun, and F. Moss for discussions, and J. Freund for manuscript comments, and the Missouri Department of Conservation for providing the paddlefish.

GRANTS

This work was supported by the Office of Naval Research, Physics Division (F. Moss), the Fetzer Institute (A. Neiman), the University of Missouri Re-

Downloaded from jn.physiology.org on June 27, 2007

search Board, and National Institute on Deafness and Other Communication Disorders Grant R01DC-04922.

REFERENCES

Amir R, Michaelis M, and Devor M. Burst discharge in primary sensory neurons: triggered by subthreshold oscillations, maintained by depolarizing afterpotentials. *J Neurosci* 22: 1187–1198, 2002.

Anishchenko VS, Astakhov VV, Neiman AB, Vadivasova TE, and Schimansky-Geier L. *Nonlinear Dynamics of Chaotic and Stochastic Systems.* Berlin: Springer-Verlag, 2002.

Anishchenko VS, Neiman AB, Moss F, and Schimansky-Geier L. Stochastic resonance: noise-enhanced order. *Physics-Uspekji* 42: 7–36, 1999.

Bade H, Braun HA, and Hensel H. Parameters of the static burst discharge of lingual cold receptors in the cat. *Pflügers Arch* 382: 1–5, 1979.

Bendat JS and Piersol AG. *Random Data: Analysis and Measurement Procedures* (3rd ed.). New York: Wiley, 2000.

Bennett MVL. Mechanisms of electroreception. In: *Lateral Line Detectors*, edited by Cahn PH. Bloomington, IN: Indiana Univ. Press, 1967, p. 313–393.

Bennett MVL and Obara S. Ionic mechanisms and pharmacology of electroreceptors. In: *Electroreception*, edited by Bullock TH and Heiligenberg W. New York: Wiley, 1986, p. 157–181.

Bialek W, Rieke F, de Ruyter van Steveninck RR, and Warland D. Reading a neural code. *Science* 252: 1854–1857, 1991.

Braun HA, Huber MT, Anthes N, Voigt K, Neiman A, Pei X, and Moss F. Interactions between slow and fast conductances in the Huber/Braun model of cold-receptor discharges. *Neurocomputing* 32: 51–59, 2000.

Braun HA, Wissing H, Schäfer K, and Hirsch MC. Oscillation and noise determine signal transduction in shark multimodal sensory cells. *Nature* 367: 270–273, 1994.

Broun GR and Govardovskii VI. Electrical model of the electroreceptor of the ampulla of Lorenzini. *Neurophysiology* 15: 166–172, 1983 (translated from *Neirofiziologiya* 15: 235–241, 1983).

Brown BR. Neurophysiology: sensing temperature without ion channels. *Nature* 421: 495, 2003.

Bullock TH. Electroreception. *Annu Rev Neurosci* 5: 121–170, 1982.

Camalet S, Duke T, Jülicher F, and Prost J. Auditory sensitivity provided by self-tuned critical oscillations of hair cells. *Proc Natl Acad Sci USA* 97: 3183–3188, 2000.

Cartwright JHE, González DL, and Piro O. Nonlinear dynamics of the perceived pitch of complex sounds. *Phys Rev Lett* 82: 5389–5392, 1999.

Chacron MJ, Longtin A, and Maler L. Negative interspike interval correlations increase the neuronal capacity for encoding time-dependent stimuli. *J Neurosci* 21: 5328–5343, 2001.

Chimento TC and Ross MD. Evidence of a sensory processing unit in the mammalian macula. *Ann NY Acad Sci* 781: 196–212, 1996.

Clusin WT and Bennett MVL. The oscillatory responses of skate electroreceptors to small voltage stimuli. *J Gen Physiol* 73: 685–702, 1979a.

Clusin WT and Bennett MVL. The ionic basis of oscillatory responses of skate electroreceptors. *J Gen Physiol* 73: 703–723, 1979b.

Crawford AC and Fettiplace R. The frequency selectivity of auditory nerve fibres and hair cells in the cochlea of the turtle. *J Physiol* 306: 79–125, 1980.

Crawford AC and Fettiplace R. The mechanical properties of ciliary bundles of turtle cochlear hair cells. *J Physiol* 364: 359–379, 1985.

Darian-Smith I, Johnson KO, and Dykes R. "Cold" fiber population innervating palmar and digital skin of the monkey: responses to cooling pulses. *J Neurophysiol* 36: 325–346, 1973.

DISLIN scientific data plotting software, available online from http://www.linmpi.mpg.de/dislin.

Dolan K, Witt A, Spano ML, Neiman A, and Moss F. Surrogates for finding unstable periodic orbits in noisy data sets. *Phys Rev E Stat Phys Plasmas Fluids Relat Interdiscip Top* 59: 5235–5241, 1997.

Douglass JK, Wilkens L, Pantazelou E, and Moss F. Noise enhancement of information transfer in crayfish mechanoreceptors by stochastic resonance. *Nature* 365: 337–340, 1993.

Eguíluz VM, Ospeck M, Choe Y, Hudspeth AJ, and Magnasco MO. Essential nonlinearities in hearing. *Phys Rev Lett* 84: 5232–5235, 2000.

Fettiplace R and Fuchs PA. Mechanisms of hair cell tuning. *Annu Rev Physiol* 61: 809–834, 1999.

Feudel U, Neiman A, Pei X, Wojtenek W, Braun H, Huber M, and Moss F. Homoclinic bifurcation in a Hodgkin–Huxley model of thermally sensitive neurons. *Chaos* 10: 231–239, 2000.

Gabbiani F and Koch C. Principles of spike train analysis. In: *Methods in Neuronal Modeling: From Ions to Networks* (2nd ed.), edited by Koch C and Segev I. Cambridge, MA: MIT Press, 1998, p. 313–360.

Gans C. An overview of the evolutionary biology of hearing. In: *The Evolutionary Biology of Hearing*, edited by Webster DB, Ray RR, and Popper AN. New York: Springer-Verlag, 1992, p. 3–13.

Geisler CD. *From Sound to Synapse: Physiology of the Mammalian Ear*. New York: Oxford Univ. Press, 1998.

Glass L. Synchronization and rhythmic processes in physiology. *Nature* 410: 277–284, 2001.

Glass L and Mackey MC. *From Clocks to Chaos: The Rhythms of Life.* Princeton, NJ: Princeton Univ. Press, 1988, chapt. 7.

Goldberg JM and Fernandez C. Physiology of peripheral neurons innervating semicircular canals of the squirrel monkey. III. Variations among units in their discharge properties. *J Neurophysiol* 34: 676–684, 1971.

Goldberg JM, Lysakowski A, and Fernandez C. Structure and function of vestibular nerve fibers in the chinchilla and squirrel monkey. *Ann NY Acad Sci* 656: 92–107, 1992.

Gummer AW. First order temporal properties of background and tone-evoked activity of auditory afferent neurons in the cochlear ganglion of the pigeon. *Hear Res* 55: 143–166, 1991.

Hegger R, Kantz H, and Schreiber T. Practical implementation of nonlinear time series methods: the TISEAN package. *Chaos* 9: 413–435, 1999. Website: http://www.mpipks-dresden.mpg.de/~tisean.

Heinz M, Schäfer K, and Braun HA. Analysis of facial cold receptor activity in the rat. *Brain Res* 521: 289–295, 1990.

Hensel H. Effect of temporal and spatial temperature gradients on the ampullae of Lorenzini. *Pflügers Arch* 347: 89–100, 1974.

Hensel H and Zotterman Y. Action potentials of cold fibres and intracutaneous temperature gradient. *J Neurophysiol* 14: 377–385, 1951.

Janson NB, Balanov AG, Anishchenko VS, and McClintock PVE. Phase synchronization between several interacting processes from univariate data. *Phys Rev Lett* 26: 1749–1752, 2001.

Jaramillo F and Wiesenfeld K. Mechanoelectrical transduction assisted by Brownian motion: a role for noise in the auditory system. *Nat Neurosci* 1: 384–388, 1998.

Jørgensen JM. The morphology of the Lorenzinian ampullae of the sturgeon *Acipenser ruthenus* (Pisces: Chondrostei). *Acta Zool* (*Stockh*) 61: 87–92, 1980.

Jørgensen JM, Flock Å, and Wersäll J. The Lorenzinian ampullae of *Polyodon spathula*. *Zellforsch Z* 130: 362–377, 1972.

Kalmijn AJ. The detection of electric fields from inanimate and animate sources other than electric organs. In: *Electroreceptors and Other Specialized Receptors in Lower Vertebrates* (*Handbook of Sensory Physiology*, vol. III/3), edited by Fessard A. Berlin: Springer-Verlag, 1974, p. 147–200.

Klinke R, Muller M, Richter CP, and Smolders J. Preferred intervals in birds and mammals: a filter response to noise? *Hear Res* 74: 238–246, 1994.

Köeppl C. Frequency tuning and background activity in the auditory nerve and cochlear nucleus magnocellularis of the barn owl *Tyto alba*. *J Neurophysiol* 77: 364–377, 1997.

Lowen SB and Teich MC. Auditory-nerve action potentials form a nonrenewal point process over short as well as long time scales. *J Acoust Soc Am* 92: 803–806, 1992.

Lu J and Fishman HM. Localization and function of the electrical oscillation in electroreceptive ampullary epithelium from skates. *Biophys J* 69: 2458–2466, 1995.

Manley GA. Preferred intervals in the spontaneous activity of primary auditory neurons. *Naturwissenschaften* 66: 582–584, 1979.

Manley GA. Evidence for an active process and a cochlear amplifier in nonmammals. *J Neurophysiol* 86: 541–549, 2001.

Manley GA, Yates GK, Kirk DL, and Köppl C. In-vivo evidence for a cochlear amplifier in the hair-cell bundle of lizards. *Proc Natl Acad Sci USA* 98: 2826–2831, 2001.

Martin P, Bozovic D, Choe Y, and Hudspeth AJ. Spontaneous oscillation by hair bundles of the bullfrog's sacculus. *J Neurosci* 23: 4533–4548, 2003.

Martin P and Hudspeth AJ. Active hair-bundle movements can amplify a hair cell's response to oscillatory mechanical stimuli. *Proc Natl Acad Sci USA* 96: 14306–14311, 1999.

Martin P, Hudspeth AJ, and Jülicher F. Comparison of a hair bundle's spontaneous oscillations with its response to mechanical stimulation reveals the underlying active process. *Proc Natl Acad Sci USA* 98: 14380–14385, 2001.

Downloaded from jn.physiology.org on June 27, 2007

Neiman AB, Russell DF, Pei X, Wojtenek W, Twitty J, Simonotto E, Wettring BA, Wagner E, Wilkens LA, and Moss F. Stochastic synchronization of electroreceptors in the paddlefish. *Int J Bifurcation Chaos* 10: 2499–2517, 2000.

Neiman A and Russell DF. Stochastic biperiodic oscillations in the electroreceptors of paddlefish. *Phys Rev Lett* 86: 3443–3446, 2001.

Neiman A and Russell DF. Synchronization of noise-induced bursts in noncoupled sensory neurons. *Phys Rev Lett* 88: 138103, 2002.

New JG and Bodznick D. Segregation of electroreceptive and mechanoreceptive lateral line afferents in the hindbrain of chondrostean fishes. *Brain Res* 336: 89–98, 1985.

Nikonov AA, Parker JM, and Caprio J. Odorant-induced olfactory receptor neural oscillations and their modulation of olfactory bulbar responses in the channel catfish. *J Neurosci* 22: 2352–2362, 2002.

Norris HW. Observations upon the peripheral distribution of the cranial nerves of certain ganoid fishes (*Amia lepidosteus*, *Polodon*, *Scaphirhyncus* and *Acipenser*). *J Comp Neurol* 39: 345–432, 1925.

Obara S and Bennett MVL. Mode of operation of ampullae of Lorenzini of the skate, *Raja. J Gen Physiol* 60: 534–557, 1972.

Ospeck M, Eguíluz VM, and Magnasco MO. Evidence of a Hopf bifurcation in frog hair cells. *Biophys J* 80: 2597–2607, 2001.

Pei X, Russell DF, Wilkens LA, and Moss F. Dynamics of the electroreceptors in the paddlefish *Polyodon spathula*. In: *Computational Neuroscience*: *Trends in Research 1998*, edited by Bower J. New York: Plenum, 1998, p. 245–249.

Pikovsky A, Rosenblum M, and Kurths J. *Synchronization: A Universal Concept in Nonlinear Science*. Cambridge, UK: Cambridge Univ. Press, 2002.

Plesser H and Geisel T. Stochastic resonance in neuron models: endogenous stimulation revisited. *Phys Rev E Stat Phys Plasmas Fluids Relat Interdiscip Top* 63: 031916, 2001.

Ratnam R and Nelson ME. Nonrenewal statistics of electrosensory afferent spike trains: implications for the detection of weak sensory signals. *J Neurosci* 20: 6672–6683, 2000.

Rosen RA and Hales DC. Feeding of paddlefish, *Polyodon spathula. Copeia* 1981: 441–455, 1981.

Rüsch A and Thurm U. Spontaneous and electrically induced movements of ampullary kinocilia and stereovilli. *Hear Res* 48: 247–263, 1990.

Russell DF, Tucker A, Wettring BA, Neiman AB, Wilkens L, and Moss F. Noise effects on the electrosense-mediated feeding behavior of small paddlefish. *Fluctuation Noise Lett* 1: L71–L86, 2001.

Russell DF, Wilkens LA, and Moss F. Use of behavioural stochastic resonance by paddle fish for feeding. *Nature* 402: 291–294, 1999.

Russell DF, Yakusheva TA, Neiman AB, and Moss F. The receptive field of an electroreceptor afferent in paddlefish corresponds to a single cluster of canals. *J Comp Physiol A Sens Neural Behav Physiol* In press.

Sand A. The function of the ampullae of Lorenzini, with some observations on the effect of temperature on sensory rhythms. *Proc R Soc Lond B Biol Sci* 125: 524–553, 1938.

Schäfer C, Rosenblum MG, Kurths J, and Abel H-H. Heartbeat synchronized with ventilation. *Nature* 392: 239–240, 1998.

Schäfer K, Braun HA, Peters RC, and Bretschneider F. Periodic firing pattern in afferent discharges from electroreceptor organs of catfish. *Pflügers Arch* 429: 378–385, 1995.

Schimansky-Geier L and Zülicke C. Harmonic noise: effect on bistable systems. *Z Phys B* 79: 451–460, 1990.

Schreiber T and Schmitz A. Improved surrogate data for nonlinearity tests. *Phys Rev Lett* 77: 635–638, 1996.

Sento S and Furukawa T. Intra-axonal labeling of saccular afferents in the goldfish, *Carassius auratus*: correlations between morphological and physiological characteristics. *J Comp Neurol* 258: 352–367, 1987.

Strogatz SH. *Nonlinear Dynamics and Chaos, With Applications to Physics, Biology, Chemistry, and Engineering.* Reading, MA: Addison-Wesley, 1994.

Suzue T, Wu GB, and Furukawa T. High susceptibility to hypoxia of afferent synaptic transmission in the goldfish sacculus. *J Neurophysiol* 58: 1066–1079, 1987.

Tass P, Rosenblum MG, Weule J, Kurths J, Pikovsky A, Volkmann J, Schnitzler A, and Freund H-J. Detection of *n*:*m* phase locking from noisy data: application to magnetoencephalography. *Phys Rev Lett* 81: 3291–3294, 1998.

Teeter JH, Szamier RB, and Bennett MVL. Ampullary electroreceptors in the sturgeon *Scaphirhynchus platorynchus* (Rafinesque). *J Comp Physiol A Sens Neural Behav Physiol* 138: 213–233, 1980.

Teich MC and Lowen SB. Fractal patterns in auditory nerve-spike trains. *IEEE Eng Med Biol* 13: 197–202, 1994.

Temchin AN. Unusual discharge patterns of single fibers in the pigeon's auditory nerve. *J Comp Physiol A Sens Neural Behav Physiol* 163: 99–115, 1988.

Teunis PFM, Bretschneider F, Bedaux JJM, and Peters RC. Synaptic noise in spike trains of normal and denervated electroreceptor organs. *Neuroscience* 41: 809–816, 1991.

Theiler J, Eubank S, Longtin A, Galdrikian B, and Farmer JD. Testing for nonlinearity in time series: the method of surrogate data. *Physica D* 58: 77–94, 1992

Tuckwell HC. *Introduction to Theoretical Neurobiology*: *Nonlinear and Stochastic Theories*, Vol. 2. Cambridge, UK: Cambridge Univ. Press, 1988.

Viancour TA. Electroreceptors of a weakly electric fish. II. Individually tuned receptor oscillations. *J Comp Physiol*133: 327–38, 1979.

Watson D and Bastian J. Frequency response characteristics of electroreceptors in the weakly electric fish, *Gymnotus carapo. J Comp Physiol* 134: 191–202, 1979.

White JA, Klink R, Alonso A, and Kay AR. Noise from voltage-gated ion channels may influence neuronal dynamics in the entorhinal cortex. *J Neurophysiol* 80: 262–269, 1998.

Wilkens LA, Russell DF, Pei X, and Gurgens C. The paddlefish rostrum functions as an electrosensory antenna in plankton feeding. *Proc R Soc Lond B Biol Sci* 264: 1723–1729, 1997.

Zahm DS. Gap junctions between sensory and supporting cells of the utricular and saccular maculae in *Anolis carolinensis* examined by transmission electron microscopy. *Am J Anat* 158: 263–273, 1980.

Zakon HH. The electroreceptive periphery. In: *Electroreception*, edited by Bullock TH and Heiligenberg W. New York: Wiley, 1986, p. 103–156.

Downloaded from jn.physiology.org on June 27, 2007